TECHNISCHE UNIVERSITÄT MÜNCHEN

LEHRSTUHL FÜR WINDENERGIE

Master's Thesis

Design of Aeroelastically Scaled Very Large Wind Turbines

Helena Canet Tarrés

WE-MT-01-10

Author: Helena Canet Tarrés
Registration number: 03669752
Professor: Carlo L. Bottasso
Supervisor: Pietro Bortolotti

Garching bei München, March 2017

Statement of Authorship

I, Helena Canet Tarrés, confirm that the work presented in this thesis has been performed and interpreted solely by myself except where explicitly identified to the contrary. All verbatim extracts have been distinguished by quotation marks, and all sources of information have been specifically acknowledged. I confirm that this work has not been submitted elsewhere in any other form for the fulfillment of any other degree or qualification.

Garching bei München, March 2017

Abstract

Wind energy has experienced an astonishing growth over the last decades and is expected to gain even more prominence in the near future. Therefore, more powerful machines are being designed, which require larger rotor diameters and higher towers to sweep larger areas and reach faster winds. The sub-scaling of those machines raises as a strong opportunity to understand the behavior of such large wind turbines due to its cost effective nature and sensorizing advantages.

This study aims at preparing the design and simulation code Cp-Max for this trend, by including new constraints to design sub-scale models capable of replicating the dynamic behavior of very large wind turbines. Furthermore, these were implemented to compare two different sub-scaling strategies: the down-zooming of a 10 MW machine and the constrained redesign of a 700 kW wind turbine.

Even though the former presented a perfect reflection of the full-scale dynamic behavior, some issues can be identified. Among these, the mismatching of the Reynolds number or manufacturing difficulties due to the thinness of several components raise doubts on the model feasibility. The latter is designed with airfoils that are more suitable to the sub-scale Reynolds number. This model was found to employ a much more realistic structure despite not yet completely matching all scaling requirements. However, these can be solved by the inclusion of more constraints into the Cp-Max environment, while the concerns identified in Z-Model can not be fixed due to the tightness of the approach.

List of Figures

List of Tables

Chapter 1

Introduction

Over the last years, renewable energies have gained prominence as an alternative to traditional energy sources. This enhancement has been partly driven by the increasing global awareness of the finite nature of traditional fossil energy sources and the potential threats of their burning to the environment. Under this context, wind power raises as a strong energy source capable of satisfying the population energy needs thanks to its enormous potential. This fact, together with its cost efficiency, partly based on low operational costs and low space needs, have motivated the impressive evolution experienced over the last decades.

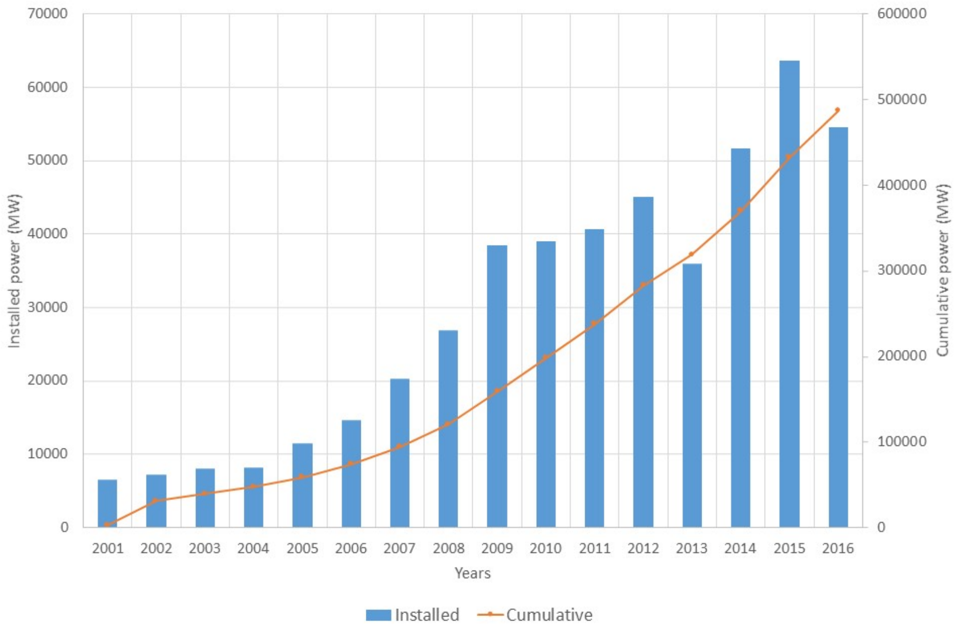

Figure 1.1: Global cumulative installed wind capacity between 2000 and 2016, data collected from [1]

This fast development has been caused by the constant installation of new wind turbines. Although at the beginning of the 21st century the yearly installed power did not experience a substantial growth, a strong incremental tendency started in 2005, as shown in Figure 1.1. A low point was reached in 2013, when only around 35,000 MW were installed, approximately 9,000 MW less than the previous year. From this point, however, the yearly installed power started to grow again, reaching a maximum value in 2015. Despite the unequal tendencies followed by the installation of power through the years, the cumulative power has never stopped rising. By 2016, almost 500,000 MW were installed, representing an increase of more than 400,000 MW in a decade.

This growth can also be associated to the better understanding of the phenomena that take part in a wind turbine that has allowed better designs. For instance, significant insight into blade aerodynamics was gained in the last decades of the 20th century thanks to the analysis of data obtained from multiple wind tunnel tests performed all over the world with models of reduced sizes given different wind conditions [11].

Among them, the Unsteady Aerodynamics Experiment (UAE) carried out at the NASA-Ames wind tunnel by the National Renewable Energy Laboratory (NREL) is particularly worth highlighting. Invaluable data was acquired from the behavior of a 10-m diameter, stall-regulated 20 kW turbine with full-span pitch control under multiple wind conditions. The comparison of the wind tunnel data against the predictions of multiple codes uncovered the importance of specific flow phenomena, such as operation in dynamic stall, 3D rotational effects or tower-wake interaction [12].

Thereafter, the improvement in measuring techniques allowed the MEXICO (Model Rotor Experiments In Controlled Conditions) project from the European Union to acquire not only data relevant to the wind turbine, but also to the surrounding air. These tests were run in the largest European wind tunnel, the DNW (German-Dutch Wind tunnel) with a 4.5-diameter wind turbine, which represented the solidity and airfoil types used on modern utility scale machines. The collected data was subsequently compared against different codes to allow their verification.

More recent studies, such as [2] expanded the goals of such tests beyond aerodynamics, also aiming at performing experimental observations in the areas of aeroelasticity and control, for single and interacting wind turbines. In addition, the testing of extreme operating conditions or advanced pitch-torque control laws was performed in a wind tunnel for the first time. To this end, a V90 wind turbine was sub-scaled into a 2-m diameter machine, shown in Figure 1.2.

Figure 1.2: Wind turbine used in the Campagnolo study, reproduced from [2].

The budding weight of wind energy has also been enabled by a rotor diameter growth. Figure 1.3 illustrates the impressive size increment that rotors have experienced in the last years: from about 15 m 30 years ago to the current rotors whose diameter is larger than 100 m. The combination of larger rotors, which allow the sweeping of a bigger area, and taller towers, which elevate the rotor to heights where the wind is blowing faster, enables the turbine to extract more power from the wind.

This tendency is set to be continued in the next years, as much effort is being devoted to the development of larger wind turbine rotors, which will allow even more power extraction from the wind, in a cost efficient way. However, the aeroelastic behavior of such large wind turbines is not yet entirely understood.

These could be captured by highly complex full-scale experiments, however not without requiring a large ability to instrument, high testing times and costs. Consequently moderate-scale machines arise as a cost-effective alternative, providing a realistic representation of large machines without presenting such significant inconveniences.

Under this context, the Scaled Wind Farm Technology Facility (SWiFT) was developed in

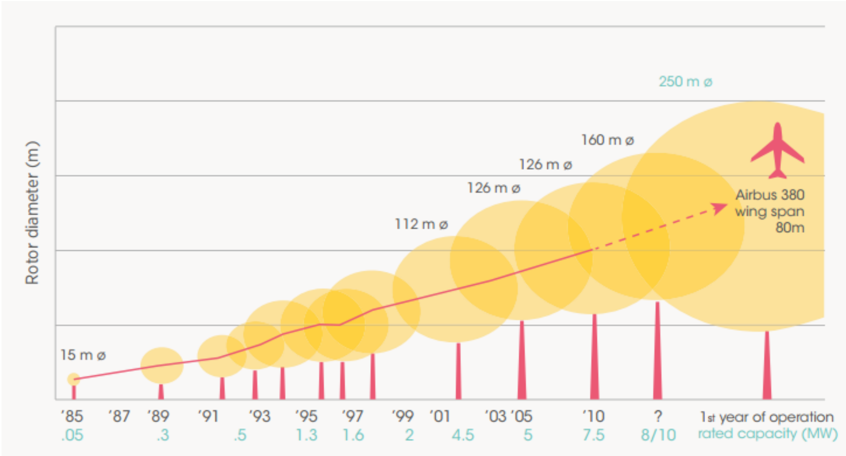

Figure 1.3: Wind turbine rotor growth, reproduced from [3]

Lubbock (Texas) by the US Department of Energy's Wind Energy Program (DOE) and Sandia National Laboratories (SNL). This field-test site, shown in Figure 1.4, is equipped with three heavily-modified 300-kW Vestas V27 wind turbines, presenting a rotor diameter of 27 m and a hub height of 31 m. Its moderate-scale has been carefully chosen to be able to reflect the behavior and performance of modern multi-megawatt machines, without presenting the inconveniences of full-scale testing. Lower blade and molds costs, as well as faster and cheaper crane scheduling and a significantly lower risk of failure motivate the need of moderate-scale testing. This facility will also provide insight into turbine to turbine interaction and wake inefficiency due to the strategically distribution of the wind turbines within the field-test site. Although it currently counts with three wind turbines, its complexity is set to increase after the installation of seven additional wind turbines over the next years.

Figure 1.4: SWiFT facility in Lubbock, Texas, reproduced from [4].

The erection of such a state-of-the-art facility represents a milestone in the wind turbine design field, as it motivates the need to develop moderate-scale blades capable of reflecting the complex behavior of larger machines. The National Rotor Testbed (NRT) will be an open-source rotor, whose design is driven by the reproduction of rotor loads and wake formation of a utility scale machine into a moderate scale blade. This redesign is being currently developed by DOE and SNL to capture the effects of a 1.5 m machine. Due to the additional constraints considered, the SWiFT blades must be scaled following a "functional scaling" [5] approach, in which the traditional geometric scaling implemented in [2] is not enough to accomplish the goals set. The replacement of the OEM blades of the SWiFT turbines by these blades, whose final design is shown in Figure 1.5, will replicate the behavior and performance of a multi-megawatt wind turbine.

A similar project, designated under the acronym WINSENT (Wind Science and Engineering

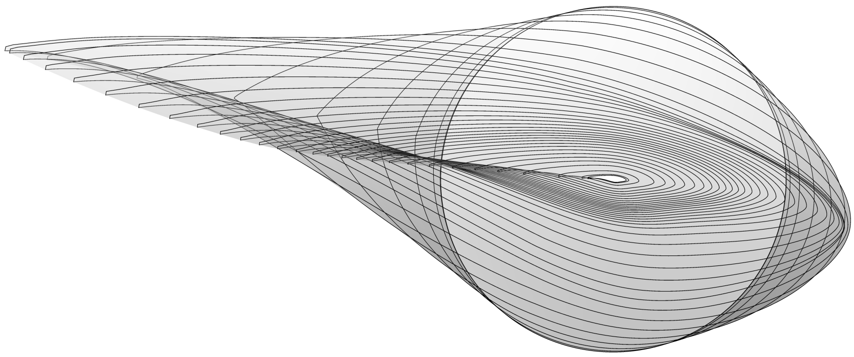

Figure 1.5: Final design of the NRT blade [5]

in Complex Terrain) is being developed in the Swabian Alps, in Germany. This site was chosen due to its particular wind conditions, as its rugged terrain creates irregular flows and turbulence. The research field-test will count with two 750 kW machines equipped with measurement sensors and state-of-the-art technology to measure in-flow and wake.
Therefore this project aims at preparing the wind turbine design and simulation code Cp-Max for this tendency. The inclusion of new constraints into the already existing aerodynamic and structural optimization algorithms will allow the design of sub-scale models capable of replicating the dynamic behavior of very large wind turbines.
Furthermore, two scaling approaches will be pursued and compared. On the one side, a zoomed-down version of a 10 MW wind turbine will be designed following the set scaling laws; while on the other side, a moderate-scale wind turbine will be redesigned with Cp-Max to reflect the dynamic behavior of this very large wind turbine.

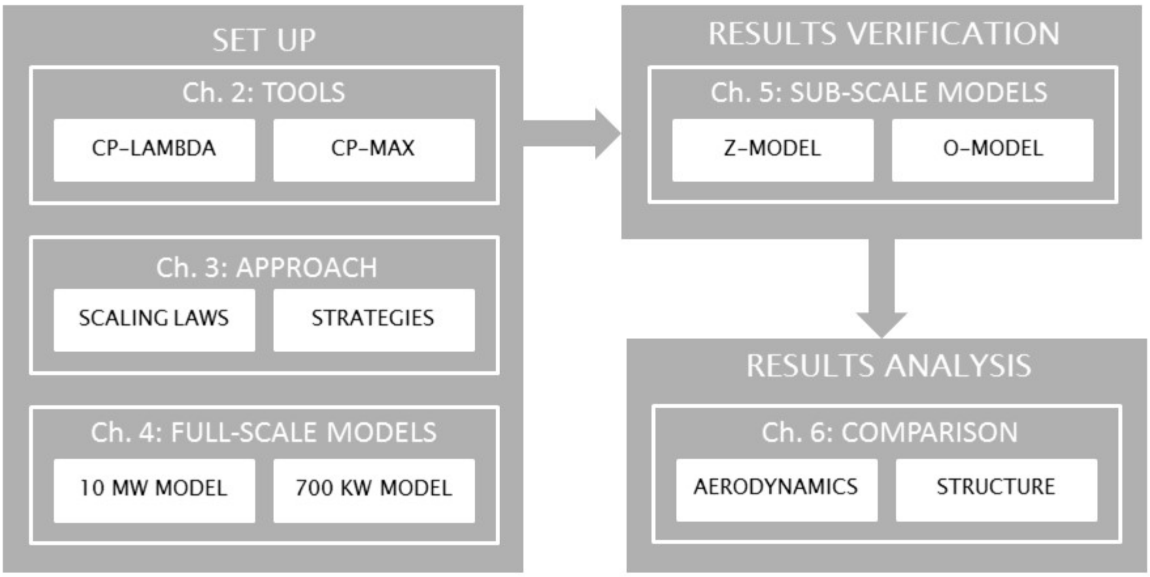

Figure 1.6: Structure of the study distributed in three different blocks, specifying the chapters included in each of them

As shown in Figure 1.6, the study is distributed in three blocks. The first one is in its turn divided into three chapters and focuses on the project setting up. It includes in Chapter 2 a description of the simulation and design tools that will be implemented, followed by an extensive explanation on the theoretical background of this study. Chapter 3 also comprises the formulation of the scaling laws that will govern the sub-scaling approaches, and the several steps that will be followed to complete them. The characteristics of the full-scale machine, the 10 MW wind turbine, that will be sub-scaled is contained in Chapter 4, as well as the main characteristics of the moderate-size wind turbine that will serve as reference for the sub-scaling.

The sub-scaling of the full-scale model into two different sub-scale machines will be performed with the tools described in Chapter 2, following the procedures described in Chapter 3. The second block therefore aims at validating the capacity of the new models of reflecting the behavior of its full-scale counterpart. This will be pursued in Chapter 5.

The similarities and differences between the models will be made clear in Chapter 6, giving special emphasis to their feasibility. A detailed summary will close this report, where the future expectations of both strategies will be explored.

Chapter 2

Tools

This chapter focuses on the multiple tools that will be implemented in this study. Therefore, the characteristics of the aeroservoelastic simulator Cp-Lambda will be detailed, as well as the optimization algorithms of the design tool Cp-Max. The codes with which these interact, ANBA and TurbSim will also be clarified. Lastly, the airfoil simulation code XFOIL will be described.

2.1 Wind turbine simulation and design tool

Wind turbine design tools are based on an aeroservoelastic simulator, which must be able to simulate the behavior of the machine with a high degree of fidelity; and a multi-disciplinary optimization algorithm, which evaluates these analyses to evaluate its figure of merit.

For this study, the multi-disciplinary research code Cp-Max (Code for Performance Maximization) was implemented, which is wrapped around the aeroservoelastic simulator Cp-Lambda [13] (Code for Performance, Loads, Aeroelasticity by Multi-Body Dynamic Analysis).

2.1.1 Cp-Lambda

The comprehensive aeroservoelastic simulator Cp-Lambda [13], which was first developed for rotorcraft applications, is based on a multi-body formulation for flexible systems with general topologies described in Cartesian coordinates. The code has been implemented in multiple industrial and research projects and validated against industrial simulation programs, wind tunnel experimental results and field measurements [6]. A large library of elements, including rigid bodies, nonlinear flexible elements, joints, actuators and aerodynamic models is available, as well as sensor and control elements, which enable the implementation of generic control laws.

The tower and rotor blades are modeled through nonlinear shear and torsion deformable beams, allowing a geometrically exact description of arbitrary-shaped beams. Joints are modeled through corresponding constraints, which are enforced by means of Lagrange multipliers. These can be equipped with elements such as internal springs, dampers, or friction, to account for such effects in the gear-box and drive-train [14].

The aerodynamic characteristics of the blade are described through lifting lines, which are based on the classical two-dimensional blade element theory. Although these are associated with beam elements, the structural reference curves are distinct, as a measure to maintain the generality of the formulation. These also include the spanwise chord and twist distributions, as well as sectional aerodynamic coefficients, stored in a look-up table given a Reynolds number and angle of attack [15].

Aerodynamic loads are computed at airstations, which are selected points along each lifting line. Each airstation is rigidly connected to an associated beam cross-section, moving with it, so that the local airflow kinematics at each airstation include the contributions due to beam movement and deformation.

Cp-Lambda implements the classical Blade-Element Momentum (BEM) theory to describe the effects of the wake, formulated according to the annular stream-tube theory with wake swirl and unsteady correction. In addition, root and blade tip losses are also taken into account, as well as unsteady aerodynamic corrections, dynamic stall, 3D blade root delayed stall and rotor-tower interference models.

2.1.2 Cp-Max

Cp-Max is a multi-disciplinary optimization algorithm aiming at minimizing the wind turbine CoE. This code is implemented within the MATLAB [16] framework, by means of the gradient-based optimization function fmincon. This optimization function implements a Sequential Quadratic Programming (SQP) algorithm, which automatically computes gradients by finite differences.

This approach is convenient because of the smoothness of the problem, which can be ensured thanks to the regular loads behavior with respect to the angle of attack due to the far-from-stall blade operation point and the smooth construction of the blade spanwise aerodynamic shape and property distributions.

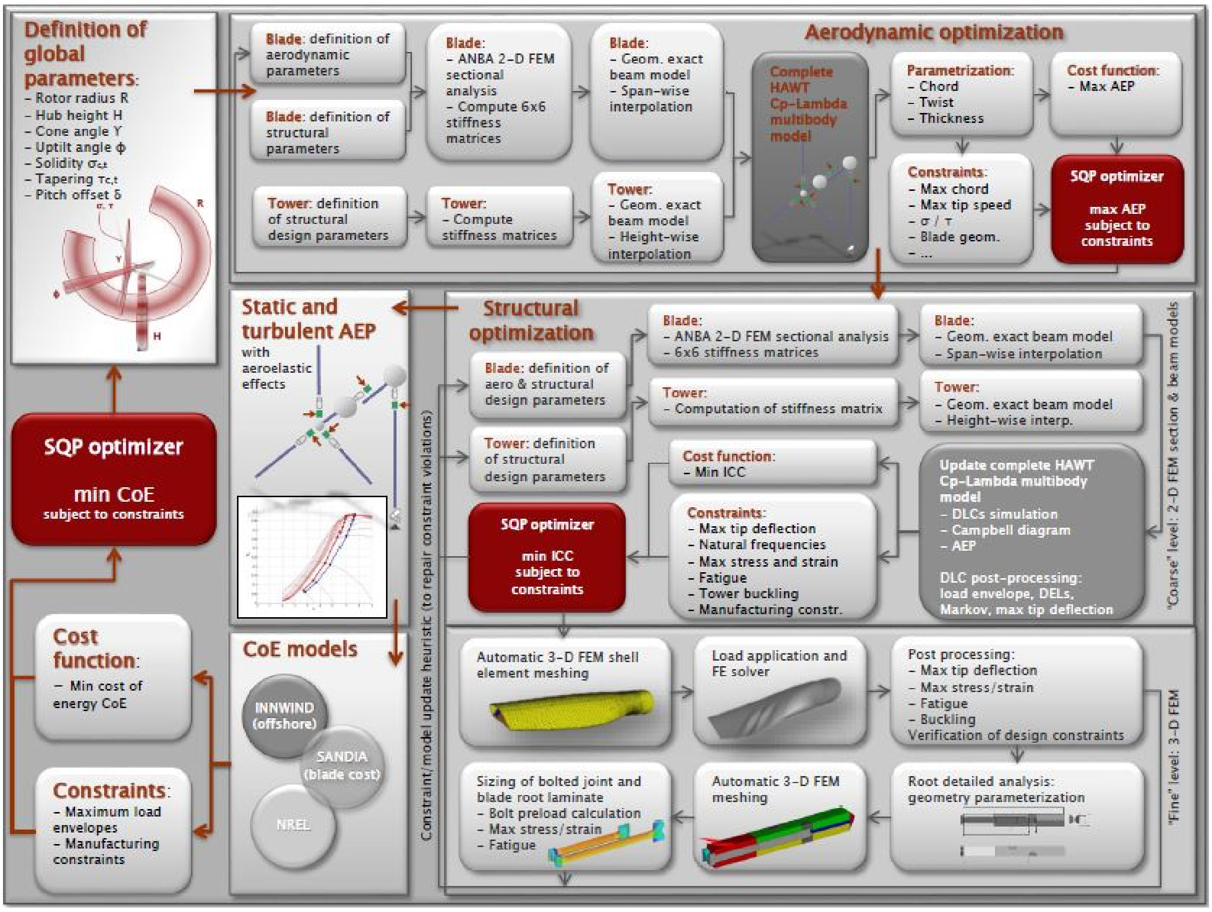

Figure 2.1: Overall scheme of Cp-Max, reproduced from [6].

Although the global optimum can not be assured, practical and realistic applications have shown that this is most likely not an important issue [15]. Figure 2.1 provides an overview into the different algorithms that form Cp-Max.

The large Cp-Max optimization can be partially executed, as it is divided in smaller optimizations: the purely aerodynamic optimization followed by a structural optimization and an aero-structural optimization, in which both optimizations are influenced.

Aerodynamic optimization

In the purely aerodynamic optimization, the structural characteristics of the blade are frozen, being only chord and twist distribution optimized for a given set of airfoils. The optimization is executed by the previously explained MATLAB [16] function fmincon, aiming at maximizing AEP under a set of both linear and nonlinear constraints. These generally include values for maximum chord, upper bounds for the first and/or second derivatives of chord and twist distributions, a tapering parameter and minimum/maximum rotor solidity values. [15].

AEP is preliminary calculated for each set of possible parameters by integrating the product of the power curve with the Weibull wind distribution for a given wind turbine class [6].

Structural optimization

The purely structural optimization aims at finding the thickness of the structural components at selected stations along the blades which minimizes the initial capital cost (ICC). This procedure is performed given a frozen rotor shape, and it can be executed for sizing the rotor for a given tower, for sizing the tower for a given rotor or for a simultaneous sizing. In this last approach, some additional constraints such as blade-tower clearance and natural frequencies placement must be considered due to the effect of each component on the other.
The search for the optimum ICC is set as an iterative loop, based on a two-level algorithm. A load analysis is performed at a first coarse level, in which a flexible beam multibody model is implemented and supplemented with 2D sectional models. The rotor and tower structural sizing is performed given a load envelope resulting from the execution of internationally standardized Design Load Cases (DLCs) [17, 18]. Fatigue damage is also estimated at this stage with a rainflow-counting algorithm.
The resulting optimal set of structural parameters is refined by means of a higher-fidelity 3D FEM analysis, which verifies the fulfillment of all the structural constraints at a finer description level, correspondingly updating them if necessary.

Integrated aero-structural optimization

The intertwining of the aerodynamic and structural loops is achieved by an outer optimization loop, whose aim is the CoE minimization. Additional non-linear constraints representing the wind turbine solidity and tapering are included in the aerodynamic loop in order to account for the mutual interaction between the two loops previously explained.

Other constraints, such as a minimum clearance between blade tip and ground, or constraints on loads can be also included in the outer loop [6].

2.1.3 TurbSim

TurbSim is a stochastic inflow turbulence tool developed to simulate randomized coherent turbulent structures. The randomized scaling of the coherent structures is based on measurements and modeled as a combination of non-homogenous Poisson and Lognormal Stochastic Processes. Therefore, a realistic representation of the spatiotemporal turbulent velocity field relationship, which are not properly reflected by the IEC Normal Turbulence Models (NTM), can be achieved. These coherent turbulent structures are superimposed on a random background turbulent field produced by a spectral model [19]. This software interacts with Cp-Max and Cp-Lambda to generate the wind conditions for the DLC cases simulated.

2.1.4 ANBA

ANBA (<u>An</u>isotropic <u>B</u>eam <u>A</u>nalysis) is a finite-element sectional code based on the theory of [20], whose discretization is performed by orthotropic isoparametric panels. Its coupling with Cp-

Lambda enables the computation of the six-by-six stiffness matrix at a selected spanwise location of the beam model. At given airfoils, blade topology, composite mechanical properties and geometry of the cross section structural members, ANBA returns fully populated matrices, which account for aeroelastic couplings due to the anisotropic composite materials. It also allows the evaluation of the stress and strain distributions on the blade sections due to the computation of recovery relationships.

2.2 Airfoil simulation tool

XFOIL [8] is an airfoil simulation tool, which can model the flow around any 2D airfoil. It can be employed as an analysis tool, as it calculates aerodynamic properties given an airfoil shape, and a Reynolds and a Mach number; or as a design tool, using inverse methods to model airfoils to achieve certain properties. Its inviscid formulation is based on a simple linear-vorticity stream function panel method, while good compressible predictions to sonic conditions are ensured by the incorporation of a Karman-Tsien compressibility correction. The wake and boundary layers are represented with a two-equation lagged dissipation integral BL formulation and an envelope e^n transition criterion.

Chapter 3

Approach

In this chapter, the theoretical framework of the sub-scaling will be explained, giving special emphasis to the scaling laws that will govern both approaches. The formulation of two scaling strategies, as well as the steps needed to pursue them will also be detailed.

3.1 Theoretical framework

The sub-scaling of any physical measurement can be justified by means of the Buckingham theorem [21]. First formulated in 1914, this theorem states that any equation involving n physical variables, which in its turn can be expressed in terms of k physical dimensions, can be represented with a set of p = n-k dimensionless parameters obtained from the original variables. Therefore sets of dimensionless parameters can be determined, even when the equation form is unknown.

This theorem can be applied to a simple model of a wind turbine, as performed by Campagnolo in [2] and summarized as follows. To this end, the tower and blades are considered as rigid bodies, being their elastic behavior introduced by springs of equivalent stiffness. Three degrees of freedom are chosen: the tower-tip fore-aft displacement x_T, the rotor azimuth ψ and the blade flapping angle φ. The description of the system can be found in Figure 3.1.

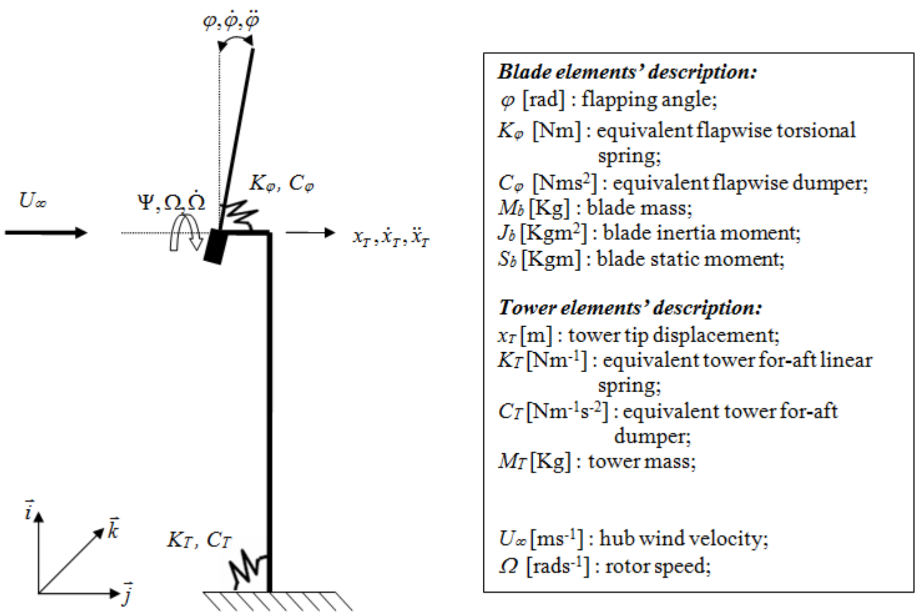

Figure 3.1: Scheme of the simplified wind turbine, reproduced from [2].

The dynamic behavior of the model can be expressed in three equations: Equation 3.1 represents the torque around the rotating axis of the turbine generated by all aerodynamic forces; equation 3.2 expresses the moment of the blade aerodynamic forces around the flapping hinge, while equation 3.3 describes the horizontal components of the aerodynamic forces.

$$J_b\left(\dot{\Omega} - 2\dot{\varphi}\varphi\Omega\right) + T_e\left(\Omega\right) = T_a\left(\mathbf{x}, \dot{\mathbf{x}}, \beta, U_\infty, B_g, \rho, \mu, a\right) \tag{3.1}$$

$$J_b\left(\ddot{\varphi} + \Omega^2\varphi\right) + \frac{1}{2}\ddot{x}_T S_b + K_\varphi \varphi + C_\varphi \dot{\varphi} = M_a\left(\mathbf{x}, \dot{\mathbf{x}}, \beta, U_\infty, B_g, \rho, \mu, a\right) \tag{3.2}$$

$$\left(M_T + M_b\right)\ddot{x}_T + \left(\ddot{\varphi} - \dot{\varphi}^2\varphi\right) S_b + C_T \dot{x}_T + K_T x_T = F_a\left(\mathbf{x}, \dot{\mathbf{x}}, \beta, U_\infty, B_g, \rho, \mu, a\right) \tag{3.3}$$

These equations not only depend on the model degrees of freedom, but also on the quantities derived, including the blade pitch β, wind velocity U_∞, the air density ρ, air viscosity μ, speed of sound a and the blade geometry, represented by means of chord c, radius R, twist Θ and airfoil shape.

The combination of these equations leads to the statement of the model dynamic equation (Equation 3.4).

$$F\left(\mathbf{x}, \dot{\mathbf{x}}, \ddot{\mathbf{x}}, M_b, M_T, J_b, S_b, K_T, C_T, K_\varphi, C_\varphi, U_\infty, \beta, B_g, t, \rho, \mu, a, g, T_e\right) = 0 \tag{3.4}$$

The dimensions of all physical quantities of this equation can be obtained as a combination of three fundamental dimensions: mass (M), length (L) and time (T), allowing the derivation of several non-dimensional parameters which will govern the wind turbine dynamics. These are summarized in Table 3.1.

Non-dimensional time	$\tau = \Omega \cdot t$
Tip-speed ratio	$\lambda = \frac{\Omega \cdot R}{U_\infty}$
Lock number	$Lo = \frac{C_{L,\alpha} \cdot \rho \cdot c \cdot R^4}{J_b}$
Non-dimensional natural frequencies	$\widetilde{\omega} = \frac{\omega_i}{\Omega}$
Mach number	$Ma = \frac{U_\infty}{a}$
Reynolds number	$Re = \frac{U_\infty \cdot c}{\nu}$
Froude number	$Fr = \frac{U_\infty{}^2}{g \cdot R}$

Table 3.1: Non-dimensional parameters relevant to the dynamic behavior of a wind turbine [2]

However, recent studies [5, 22] suggest that the near-wake structure is closely influenced by the blade circulation distribution. The high dependency between wake stability and circulation distribution has been concluded from high-fidelity CFD solutions, which suggest that the same wake structure can be achieved when the same circulation distribution is found.

Circulation represents the rotation of the wind originated due to the opposed torque that the rotor exerts upon the wind after it passes through. Its mathematical description, shown in Equation 3.5, interprets circulation as the macroscopic measure of the rotation of the wind for a finite area of the fluid [23], where u is the velocity component in the flow direction x; and v represents the component in the direction perpendicular to the flow.

$$\Gamma = \int\int \left(\frac{\partial u}{\partial y} - \frac{\partial v}{\partial x}\right) dx dy \tag{3.5}$$

Nevertheless, it is useful to define the dimensionless circulation (Equation 3.6) to allow the comparison between rotors of different scales.

$$\Gamma'\left(\frac{r}{R}\right) = \frac{\Gamma(\frac{r}{R})}{R \cdot U_\infty} = \frac{C_L}{2} \cdot \frac{V_{rel}}{U_\infty} \cdot \frac{c}{R} \tag{3.6}$$

where: C_L is the lift coefficient; V_{rel} the airfoil section air speed; U_∞, the wind inflow speed; c the blade chord, r the local rotor radius and R the rotor radius.

The blade deflection can also be implemented to characterize the ratio between aerodynamic and elastic forces. When the blade is regarded as a cantilever beam, with one end anchored and the other one free where a load is applied, it deforms proportionally to the ratio between aerodynamic forces (F) and elastic forces (k), as displayed in equation 3.7.

$$\delta = \frac{F}{k} \tag{3.7}$$

3.1.1 General scaling requirements

It is impossible to design a sub-scale model that exactly matches all the non-dimensional quantities stated in Table 3.1. Hence it is essential to choose scaling laws that ensure the appropriate scaling of inertial, elastic and aerodynamic behavior despite the mismatch of some of these quantities. These are stated as follows:

- Non-dimensional time must be the same between models to avoid disturbances of the system dynamic response.
- The tip-speed ratio must be kept constant to ensure the same kinetic behavior.
- The dimensionless circulation of the sub-scale model must be the same of its full-scale counterpart to ensure the same wake behavior.
- The deflections of the sub-scale model must match the one of its counterpart to ensure the same ratio between aerodynamic and elastic forces.
- The ratio of elastic to inertial forces must be locked by keeping the same non-dimensional natural frequencies, leading to the same excitation and natural frequencies placement.
- Incompressible flow ($Ma \leq 0.3$) must be ensured to neglect the effect caused by Mach number differences.
- Despite the impossibility of maintaining the same Reynolds number, its mismatching should be minimized.

3.2 Scaling strategies

Two different strategies will be pursued, whose characteristics are shown in Figure 3.2. On the one side, a full-scale model will be zoomed down into a sub-scale model, from now on designated Z-Model; while on the other side, a wind turbine of moderate scale will be redesigned to match the requirements of the full-scale wind turbine previously stated. The main difference between the models lies on the choice of airfoils, as the down-zooming nature of the Z-Model requires the implementation of the same airfoils as its full-scale counterpart. For the O-Model, however, another set of airfoils can be chosen.

3.2.1 Z-Model

The Zoomed-Down Model (Z-Model) is designed as an scaled exact replica of the full-scale machine. As previously stated, all wind turbine characteristics can be expressed on terms of mass (M), length (L) and/or time (T). Therefore the formulation of a mass, length and time scaling ratio is enough to determine all sub-scale wind turbine characteristics.
To this end, the rotor diameter ratio between the full-scale (represented in the equations by the

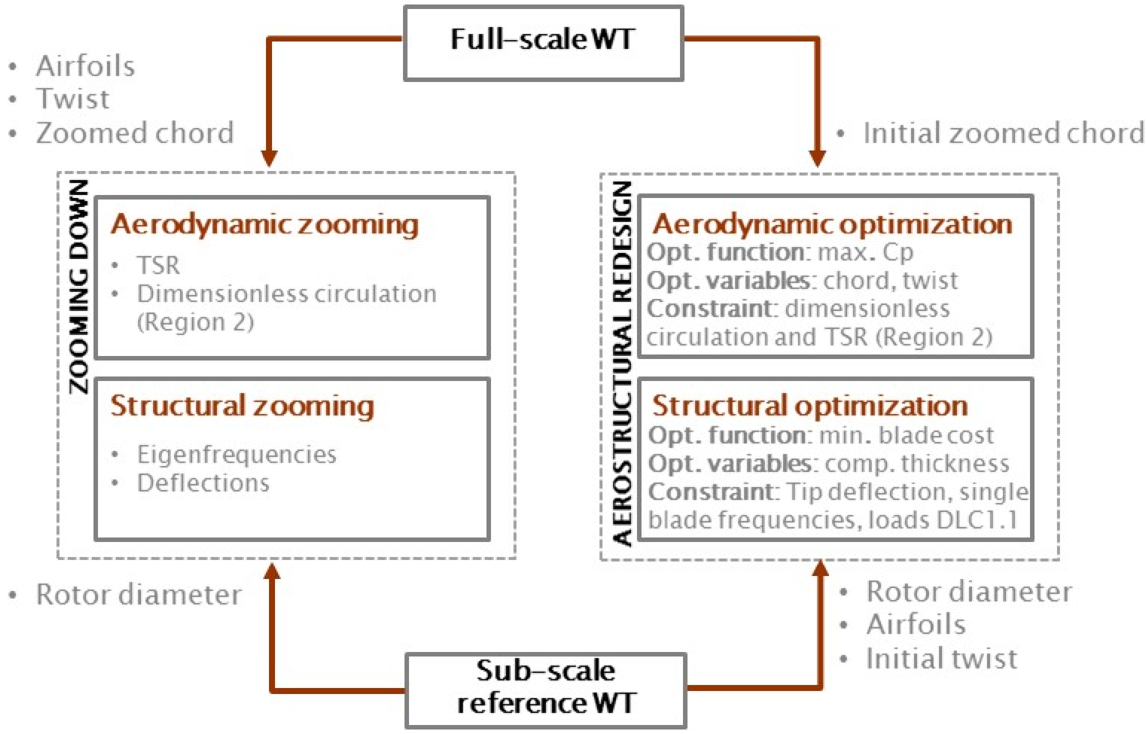

Figure 3.2: Overview of the scaling strategies that will be compared

subscript f) and the sub-scaled model (symbolized by the subscript s) determines the length scaling ratio; while the time scaling ratio η_t, is set by the time scale (Equation 3.9) in each model. Furthermore the ratio of rotor speeds must be equal to the time scaling factor to ensure the same non-dimensional time ($\tau = \Omega \cdot t$), as formulated in the scaling laws.

$$\eta_g = \frac{R_s}{R_f} \tag{3.8}$$

$$\eta_t = \frac{T_s}{T_f} = \frac{\omega_f}{\omega_s} \tag{3.9}$$

The mass scaling ratio can be determined by a combination of the length and time scaling ratios, due to the fact that the air density can not be scaled (Equation 3.10), imposing a ratio between masses and lengths between both models.

$$\rho_s = \rho_f \tag{3.10}$$

This equality (Equation 3.10) can be translated into a mass/length ratio when regarded by its units, as expressed in equation 3.11.

$$\left[\frac{kg}{m^3}\right]_s = \left[\frac{kg}{m^3}\right]_f \tag{3.11}$$

The mass ratio between the full-scale and sub-scale models can thus be set (Equation 3.12).

$$\left[\frac{kg_s}{kg_f}\right] = \left[\frac{{m_s}^3}{{m_f}^3}\right] = {\eta_g}^3 \tag{3.12}$$

These ratios serve as a base to determine the scaling parameters of all wind turbine features, summarized in Table 3.2.

Wind turbine configuration		
Feature	**Magnitude**	**Scaling ratio**
Rotor Diameter	L	η_g
Hub height	L	η_g
Rotor Cone Angle	-	-
Nacelle Uptilt Angle	-	-
Rotor Overhang	L	η_g
Length Blade Root Flange	L	η_g
Blade aerodynamic characteristics		
Feature	**Magnitude**	**Scaling ratio**
Chord	L	η_g
Twist	-	-
Relative thickness	-	-
Airfoil characteristics	-	-
Blade and tower structural characteristics		
Feature	**Magnitude**	**Scaling ratio**
Blade and tower components thickness	L	η_g
Blade topology position	L	η_g
Axial and Shearing stiffness	$M \cdot L \cdot T^{-2}$	$\eta_g^4 \cdot \eta_t^{-2}$
Bending and torsional stiffness	$M \cdot L^3 \cdot T^{-2}$	$\eta_g^6 \cdot \eta_t^{-2}$
Non-structural masses	$M \cdot L^{-1}$	η_g^2
Wind turbine control		
Feature	**Magnitude**	**Scaling ratio**
Rated Omega	T^{-1}	${\eta_t}^{-1}$
Rated TSR	-	-
Maximum tip speed	$L \cdot T^{-1}$	$\eta_g \cdot {\eta_t}^{-1}$
Cut-in and Cut-out wind speeds	$L \cdot T^{-1}$	$\eta_g \cdot {\eta_t}^{-1}$

Table 3.2: Scaled features of the Z-Model, where M represents mass; L, length and T, time

Model validation

The model must be validated to ensure that it presents the same dynamic behavior as its full-scale counterpart. To this end, it must be proved, that all scaling laws listed in Chapter 3.1.1 are correctly fulfilled. An overview of the model validation is displayed in Table 3.3.

VALIDATIONS			
Validation	**Feature**	**Magnitude**	**Scaling factor**
Kinetic behavior	TSR	-	-
Aerodynamic forces	Dimensionless circulation	-	-
Elastic forces	Deflection	L	η_g
Inertial forces	Frequency placement	T^{-1}	${\eta_t}^{-1}$

Table 3.3: Conditions to be fulfilled for the Z-Model

The kinetic behavior of the sub-scale machine will be equal to the full-scale on if the TSR is kept constant. Furthermore, the aerodynamic forces will be correctly scaled if the new model presents the same dimensionless circulation. Elastic and inertial forces can be proved by respectively checking the blade deflection and the frequency placement, which must be correctly scaled.

Moreover, it is necessary to ensure the incompressibility of the air, in order to be able to neglect the Mach number mismatching; while the sub-scale model Reynolds number should not present large differences with its full-scale counterpart, as this may influence the airfoil properties, effecting their aerodynamic behavior.

The scaled dynamic behavior of the Z-Model can only be ensured when all these conditions are fulfilled.

3.2.2 O-Model

In the optimized model (O-Model) a blade will be designed, whose behavior matches that of the full-scale wind turbine. To this end, an already existing wind turbine will be chosen and correspondingly redesigned, according to the constraints fixed.

Model constraints

The wind turbine simulation and design tool Cp-Max described in Chapter 2.1.2 will be implemented to design the O-Model. This code already counts with aerodynamic and structural optimization loops that enable an optimal design. However, additional constraints, listed in Table 3.4, must be introduced to ensure the scaling of the full-scale wind turbine behavior.

Constraints to match the TSR in Region 2 and the dimensionless circulation of the full-scale model are thus included into the aerodynamic optimization algorithm. Therefore, the code will look for a blade aerodynamic shape that not only offers the maximum Cp, but also shows the desired dimensionless circulation at the set TSR. These depend on the wind turbine structural characteristics as aeroelastic interactions take place, being subsequently necessary to suppress these effects by running the first iteration under the consideration of a rigid blade.

The structural loop must be constrained to ensure the matching of elastic and inertial behavior. Therefore, restrictions on first flapping and lagging mode and tip displacement are included. The code will then determine the optimal components thicknesses given a certain topology that match these restrictions and are able of withstanding the loads obtained in the basic dynamic loads cases (DLC 1.1).

Design restrictions				
Optimization	**Constraint**	**Feature**	**Magnitude**	**Scaling factor**
Aerodynamic	Kinetic behavior	TSR	-	-
Aerodynamic	Aerodynamic	Dimensionless circulation	-	-
Structural	Elasticity	Deflection	L	η_g
Structural	Inertia	Frequency placement	T^{-1}	${\eta_t}^{-1}$

Table 3.4: Constraints placed on the aerodynamic and structural loop to design a sub-scale turbine matching the dynamic behavior of its full-scale counterpart

The optimal O-Model will be achieved after several iterations between these loops.

Chapter 4

Full-scale models

In this chapter, the full-scale wind turbine that will be sub-scaled will be described. In addition, the main characteristics of the modern-size wind turbine used as a reference for the sub-scale machines will be included.

4.1 10 MW Model

The 10 MW machine described in [15] is the model chosen to represent the very large wind turbines that will be scaled. Based on the DTU 10 MW [9] research wind turbine, which was developed by Danmarks Tekniske Universitet (DTU), this model was created at Technische Universität München (TUM), presenting multiple structural and aerodynamic variations.
Under the included improvements, different structural changes as well as an extra rotor cone angle can be found. These result of the additional conditions considered, such as maximum thickness and tapering rates of laminates to translate manufacturing and technological constraints, as well as blade-tower clearance, ultimate stress, ultimate strain and fatigue damage.
The new configuration was achieved after the model simulation with the aeroservoelastic simulator Cp-Lambda described in Chapter 2.1.1, and a multi-level mono-disciplinary structural optimization carried out with Cp-Max, whose algorithms are briefly clarified in Chapter 2.1.2.

4.1.1 Main characteristics

This machine has been designed for sittings with high winds and high turbulence, being classified in 1A wind class. The design of this machine is strongly influenced by this consideration, as a trade-off between a good aerodynamic performance and a load-resistant structure must be achieved.
Among the main characteristics summarized in Table 4.1, the large dimensions of the machine, such as the rotor diameter of 178.3 m or the high hub height of 119 m stand out.

Data	Value	Data	Value
Wind class	IEC 1A	Rated mech. power	10.00 MW
Hub height	119.0 m	Rotor diameter	178.3 m
Rotor cone	4.65 ^{o}	Nacelle uptilt	5.0 ^{o}
Rotor overhang	7.07 m	Length Blade Root Flange	2.8 m
Rotor solidity	4.66 %	Max V_{tip}	$90\,\mathrm{m}\cdot\mathrm{s}^{-1}$
Blade mass	42.496 kg	Tower mass	628.0 t
Cut-in wind speed	$4\,\mathrm{m}\cdot\mathrm{s}^{-1}$	Cut-out	$25\,\mathrm{m}\cdot\mathrm{s}^{-1}$

Table 4.1: Configuration of the 10 MW offshore wind turbine [6]

4.1.2 Aerodynamic characteristics

The blade external shape is characterized by the chord, twist and relative thickness distribution along the blade. These are plotted in Figure 4.1 over non dimensional blade span. The chord (Figure 4.1a) displays a conventional decreasing tendency, reaching its maximum value of approximately 6 m around a normalized radius of 0.27. The aerodynamic twist (Figure 4.1b) presents a constant value at the root and starts decreasing when the chord starts increasing. The twist distribution is set to maximize the power extraction of the wind turbine, by allowing all airfoils to operate at optimal angle of attack.

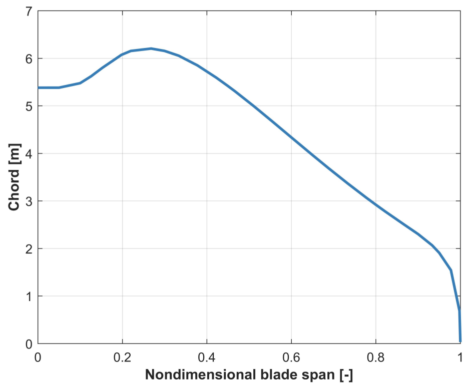

(a) Chord distribution

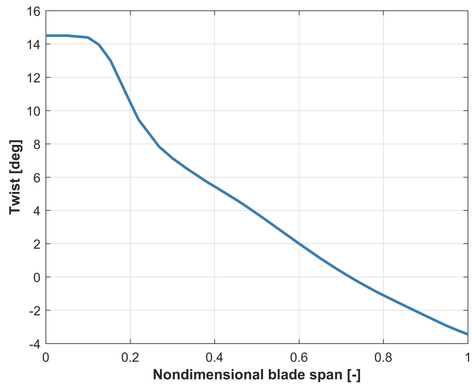

(b) Twist distribution

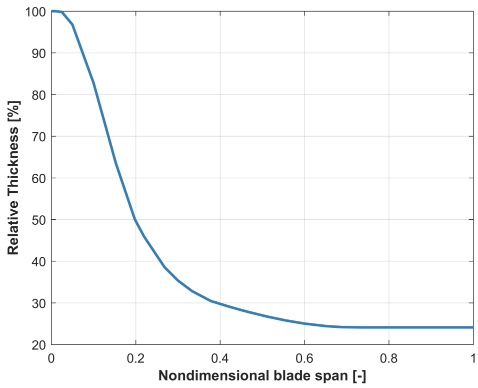

(c) Relative thickness distribution

Figure 4.1: Chord, twist and relative thickness distribution along the 10 MW wind turbine blade

The blade relative thickness decreases along the blade span to account for the section-specific structural and aerodynamic requirements: the lower structural loads towards the tip allow the implementation of thinner, and thus more efficient airfoils.

Airfoils

This distribution is defined by the placement of airfoils of 48 %, 36 %, 30.1 % and 24.1 % thickness of the FFA-W3 series, whose geometry is shown in Figure 4.2.

The airfoil aerodynamic properties were set by running 2D CFD calculations between angles of attack of -32° and 32°. These were computed at Reynolds numbers between 6×10^7 and 1.2×10^7 due to the large dimensions of the rotor. 3D corrections were performed applying the model developed in [24] and completed to the whole angle of attack range [9]. The resulting curves are shown in Figure 4.3 and implemented in this model.

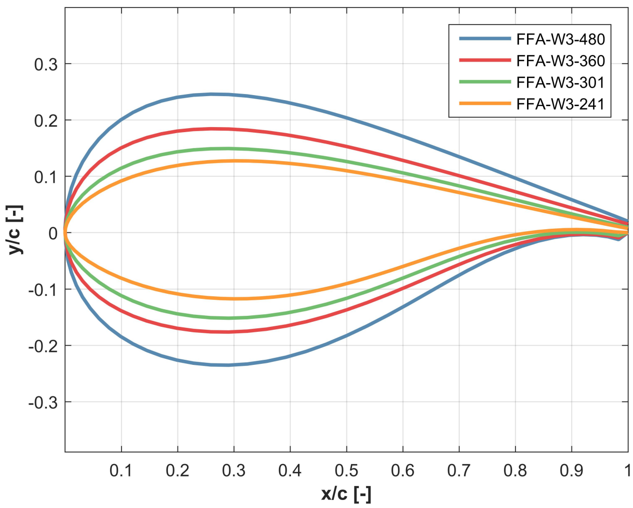

Figure 4.2: Geometry of the FFA-W3-XXX airfoil family employed in the 10 MW wind turbine

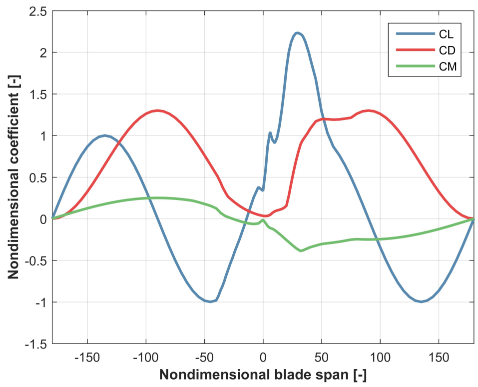

(a) FFA-W3-480 at $Re = 1 \times 10^7$

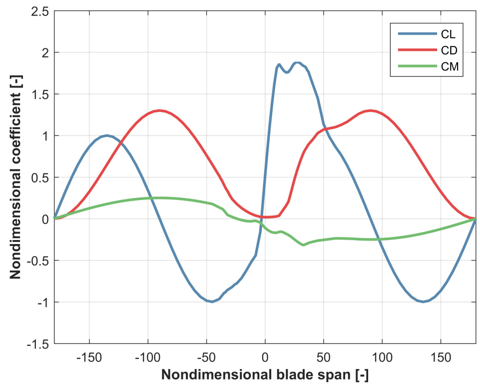

(b) FFA-W3-360 at $Re = 1 \times 10^7$

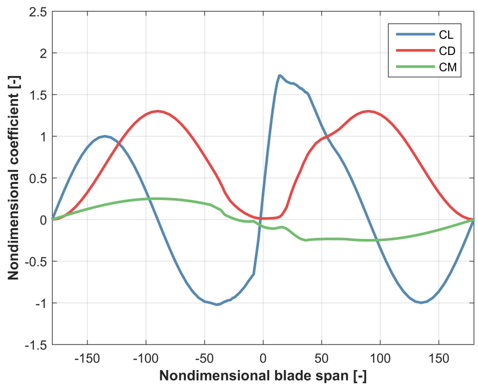

(c) FFA-W3-301 at $Re = 1 \times 10^7$

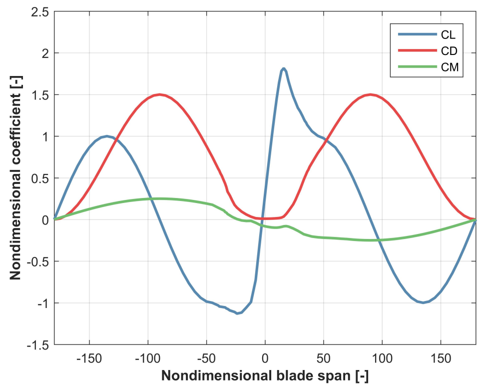

(d) FFA-W3-241 at $Re = 1.2 \times 10^7$

Figure 4.3: Aerodynamic properties of the different airfoils

4.1.3 Campbell Diagram

The possible resonant conditions can be analyzed with the Campbell diagram. In this diagram the modes natural frequencies are represented, allowing the identification of potential dangerous situations. These can take place when multiple modes are found at the same natural frequency, as energy is transferred from one mode into the other, or in crossings between natural frequencies and P-harmonics, as external energy is introduced into the response.

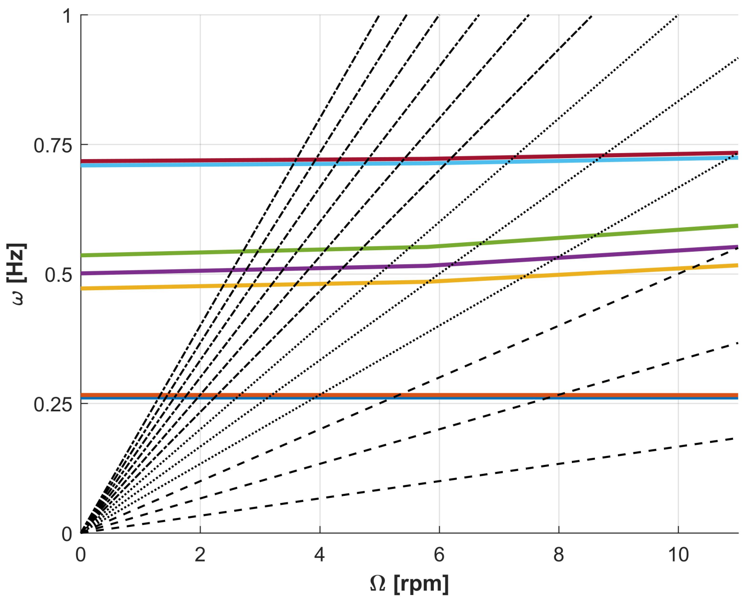

Figure 4.4: 10 MW wind turbine Campbell diagram

The Campbell diagram of the 10 MW machine is shown in Figure 4.4.

4.1.4 Cp-Lambda Diagram

The Cp-Lambda Diagram depicts the behavior of the Cp of the wind turbine blade at different TSR and a constant pitch, as shown in Figure 4.5.

The maximum Cp has a value of 0.4620 and is reached at a TSR of 7.684 and pitch of 0.0055 ^{o}, as summarized in Table 4.2.

Data	Value
TSR [-]	7.684
Pitch [deg]	0.0055
Cp [-]	0.4620
Ct [-]	0.7916

Table 4.2: Description of the conditions of Region 2 in the 10 MW model

4.1.5 Control laws

The 10 MW wind turbine is controlled through a variable-speed collective pitch strategy with a maximum tip speed constraint of $90\,\mathrm{m \cdot s^{-1}}$. The regulation strategy followed by the wind

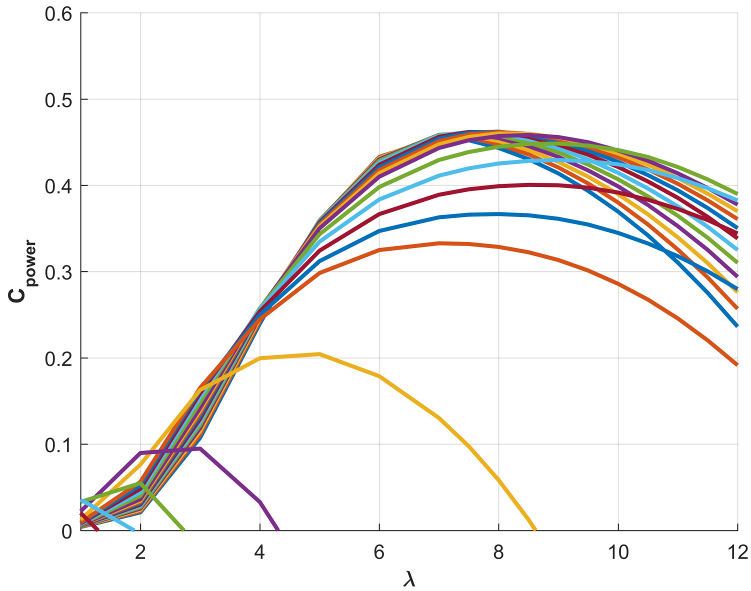

Figure 4.5: Cp-Lambda diagram of the 10 MW wind turbine

turbine is represented in Figure 4.6, where the control regions can be distinguished. These can be defined according to the power, torque, pitch and rotor speed behavior in each one of them.

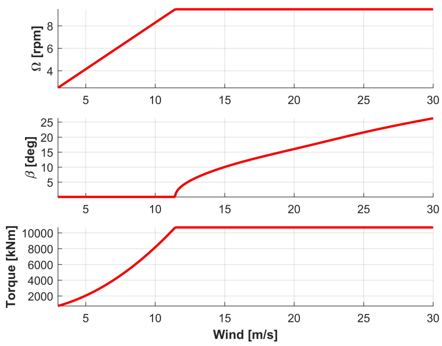

(a) Pitch, Torque and Omega control

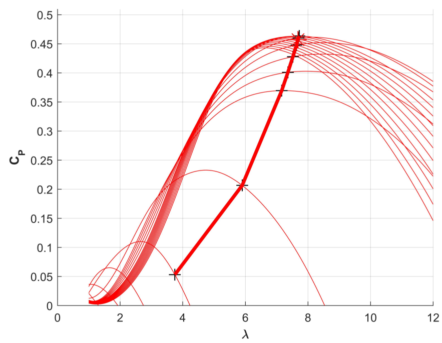

(b) Regulation trajectory

Figure 4.6: Regulation strategy of the 10 MW wind turbine

In Region 1, the wind turbine does not operate as the the wind speeds are below cut-in speed, being too weak to produce power.
Region 2 comprises wind speeds from cut-in up to rated speed, in which the wind turbine operates at its maximum power coefficient, and thus, constant TSR. To maintain this operational point, the rotor speed must adapt to the wind speed, while pitch is kept constant. Under these conditions, torque and power will correspondingly grow until reaching their rated values.
The control above rated speed, known as Region 3, aims at maintaining the power at its rated value. This condition implies the need to keep torque and rotor speed constant. The machine is then regulated by pitching to adapt the TSR to the new wind speed. This control strategy does not require the definition of a Region 2 1/2 as the maximum tip speed achieved is $88.35\,\mathrm{m}\cdot\mathrm{s}^{-1}$, lower than the maximum tip speed constraint.

4.1.6 Dimensionless circulation

The blade dimensionless circulation is computed in Region 2, where the wind turbine operates at its maximum Cp. This region corresponds to the point, whose operating conditions have been summarized in Table 4.2. An increasing tendency can be identified from the root to a nondimensional blade span of around 0.3, where the maximum value is reached. After mostly maintaining a constant value through the blade span, it starts decreasing when approaching the blade tip, as displayed in Figure 4.7.

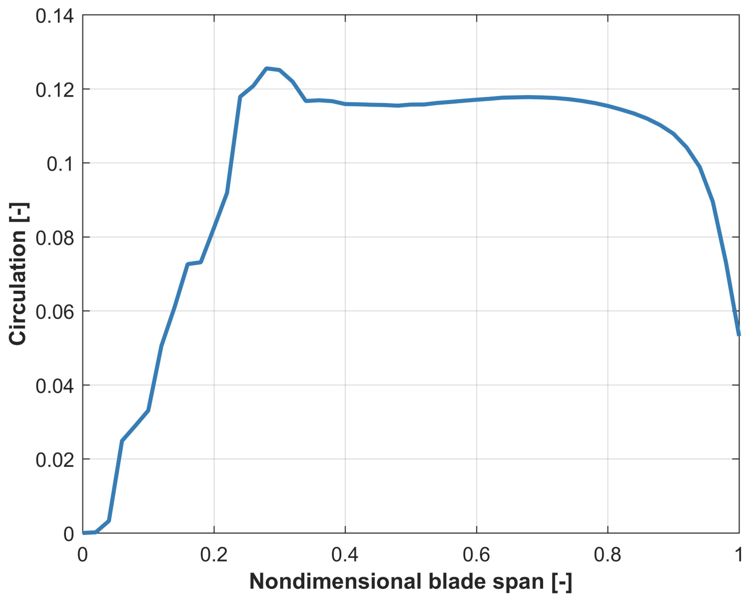

Figure 4.7: Dimensionless circulation along the 10 MW blade

4.1.7 Deflection

For the computation of the blade deflection, a cantilever beam with a force applied on the free end is considered. The deflection of the blade given different forces is displayed in Figure 4.8.

4.2 700 kW Model

The 700 KW Model is based on the GARUDA 700.54 wind turbine [10], whose main characteristics are summarized in Table 4.3. As it wind class suggests, this wind turbine has been designed for sittings presenting low wind speeds. Therefore the machine characteristics, such as the diameter of 54 m or the hub height of 73 m have been influenced by this condition.

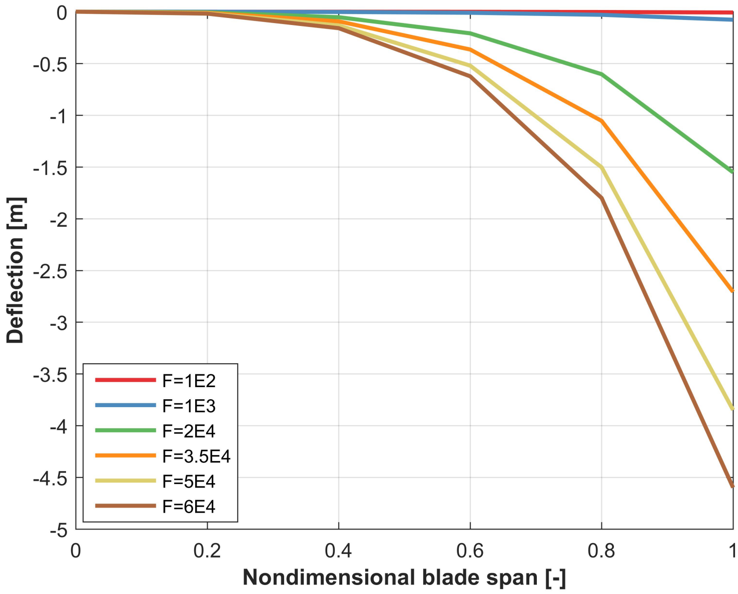

Figure 4.8: Deflection of the blade considered as a cantilever

Data	Value	Data	Value
Wind class	IEC 3A	Rated mech. power	700.0 kW
Hub height	73 m	Rotor diameter	54.00 m
Rotor cone	2.50 ^{o}	Rotor overhang	3.07 m
Length Blade Root Flange	0.65 m	Rated rotational speed	26.5 rpm
Cut-in wind speed	$3.5\,m \cdot s^{-1}$	Cut-out	$24\,m \cdot s^{-1}$

Table 4.3: Configuration of the 700 kW wind turbine [10]

Chapter 5

Sub-scale models

Two sub-scale models will be designed following the approaches shown in Figure 3.2 from a full-scale model, the 10 MW wind turbine characterized in Chapter 4.1, and a moderate-size reference wind turbine, the 700 kW model, whose characteristics were exposed in Chapter 4.2. Both models aim at reflecting the same dynamic behavior as their counterpart, however under different design methods. In this chapter, the building and validation of the models will be performed.

5.1 Z-Model

The down-zoomed model will be set following a pure-scaling approach, in which all features are correspondingly scaled. After the model set-up, the behavior of the model must be verified against the full-scale model, following the methodology unfolded in Chapter 3.2.1.

5.1.1 Model set-up

Z-Model is based on the length, time and mass scaling ratios, defined by the characteristics of the full- and sub-scale models, which determine the relation between all features, as demonstrated in Table 3.2. As commented in Chapter 4.1, the initial 10 MW machine presents a diameter of 178.3 m, while the diameter of the sub-scale machine is of 54.0 m, as established in Chapter 4.2. Therefore, the length scaling factor can be set as the ratio between these values (Equation 5.1).

$$\eta_g = \frac{R_s}{R_f} = \frac{54.0}{178.3} = 0.3029 \tag{5.1}$$

The mass scaling ratio directly depends on the length scaling ratio, as demonstrated in Chapter 3, while the time scaling ratio can be freely chosen. The relatively large size of the sub-scale model allows the setting of the time scaling ratio equal to the length one, as no control bandwidth problems are foreseeable under this condition. Therefore, TSR will automatically match and velocities are kept constant between models. This model is consequently set with a sub-scaled chord $c_s = \eta_g \cdot c_f$, but the same twist and airfoil characteristics and position as its full-scale counterpart. The main blade shape characteristics are shown in Figure 5.1.

Due to its purely zoomed-down nature, properties of parts of the wind turbine which do not correspond to the rotor, such as the root flange, the nacelle or the hub are also zoomed following the same scaling factors. Consequently, the new model presents the same solidity as its full-scale counterpart.
Other structural properties, such as stiffnesses and structural components are correspondingly scaled following Table 3.2.

5.1.2 Model validation

The validation steps for the Z-Model were set in Chapter 3.2.1 as a way of ensuring the similarity between the dynamic behavior of this model and that of its full-scale counterpart.

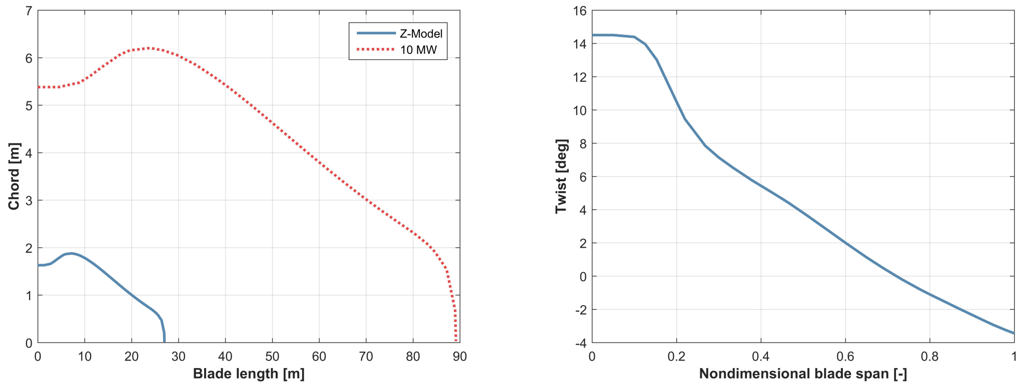

(a) Chord distribution (b) Twist distribution

Figure 5.1: Chord and twist distribution along the Z-Model turbine blade

Data	Value	Data	Value
Wind class	IEC 3A	Rated mech. power	700.00 kW
Hub height	36.04 m	Rotor diameter	54.0 m
Rotor cone	4.65 ^{o}	Nacelle uptilt	5.0 ^{o}
Rotor overhang	2.14 m	Length Blade Root Flange	0.85 m
Rotor solidity	4.66 %	Max V_{tip}	$90\,\mathrm{m \cdot s^{-1}}$
Cut-in wind speed	$4\,\mathrm{m \cdot s^{-1}}$	Cut-out	$25\,\mathrm{m \cdot s^{-1}}$

Table 5.1: Z-Model main characteristics

In Figure 5.2 the dimensionless circulation of the Z-Model is displayed and compared against that of the 10 MW wind turbine. This is represented in Region 2, point where the Cp reaches its maximum. The dimensionless circulation of the Z-Model is a perfect replica of that from the 10 MW wind turbine, suggesting the same aerodynamic behavior.

In addition, the Cp and Ct of the Z-Model do not differ much from the values of the 10 MW model, as seen in Table 5.2. The Z-Model should present the same Cp, as the same airfoils as

Data	10 MW	Z-Model
TSR [-]	7.684	
Pitch [deg]	0.0055	
Cp [-]	0.4620	0.4621
Ct [-]	0.7916	0.7911

Table 5.2: Comparison between Region 2 in the 10 MW model and in Z-Model

in its full-scale counterpart are being employed, while the same Ct implies that the surrounding air experiences the same velocity deficit.

However, the Reynolds number of the Z-Model is much smaller than the one of the 10 MW model, as demonstrated in Figure 5.3. This may have an effect on the airfoils properties, which may lead to a different circulation distribution. The validation of the elastic forces is carried out by the comparison of the deflection of the model given the application of different forces on one

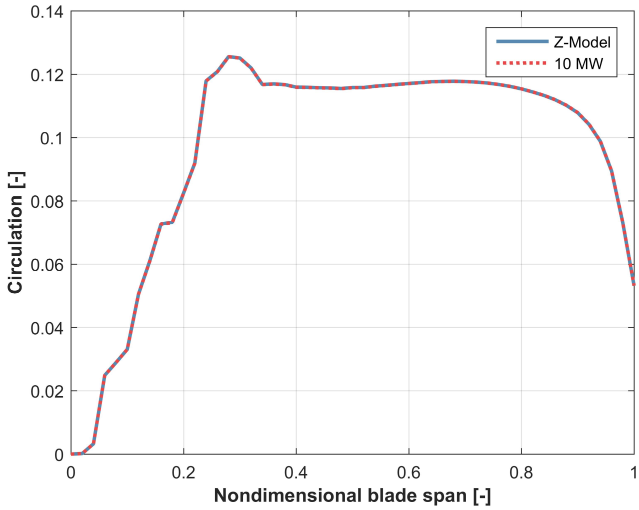

Figure 5.2: Comparison of the circulation in Region 2 of the Z-Model and the 10 MW model

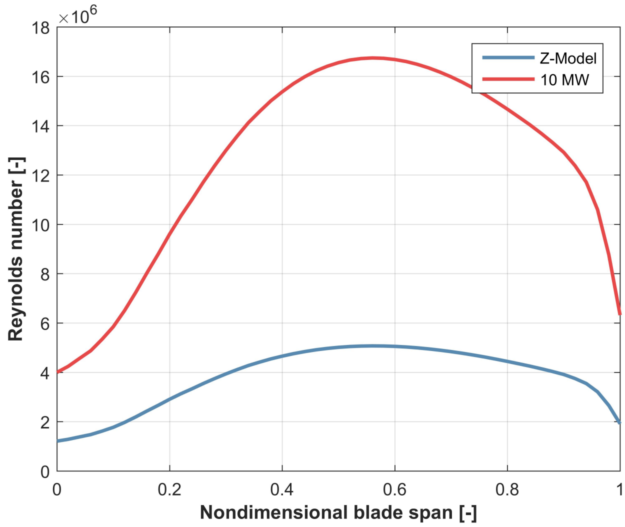

Figure 5.3: Comparison of the Reynolds number of the Z-model and the 10 MW wind turbine

blade's end. In Figure 5.4, it is clear how the Z-Model behaves like the 10 MW Model when scaled forces are applied, validating the similarity of the elastic forces.

For the validation of the inertial forces similarity, the eigenfrequencies of the models are compared. The Campbell diagram of both models is displayed in Figure 5.5, in which the similarity at low rotational speeds is obvious. Both the single blade modes, as the rotor-as-a-whole eigenfrequencies are therefore correctly scaled.

5.2 O-Model

The O-Model will be set following a constrained aerostructural optimization in Cp-Max. The initial characteristics of the model and the results of its optimization will be commented as follows.

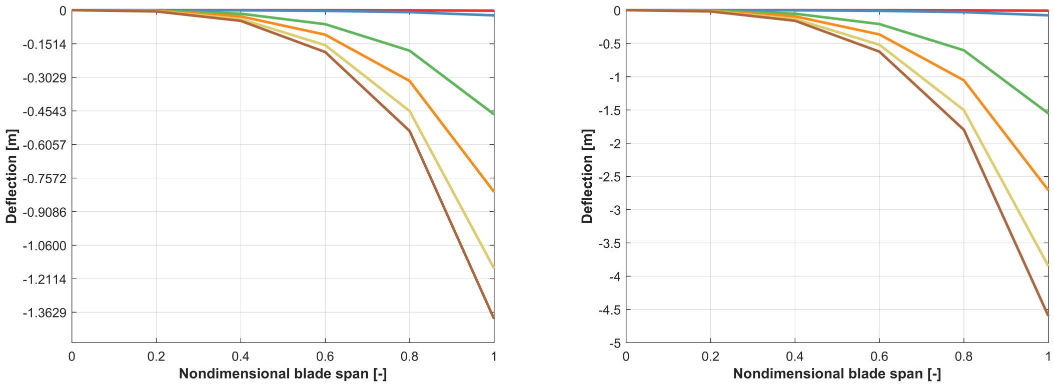

(a) Z-Model (b) 10 MW Model

Figure 5.4: Comparison of the deflections of the 10 MW Model and the Z-Model

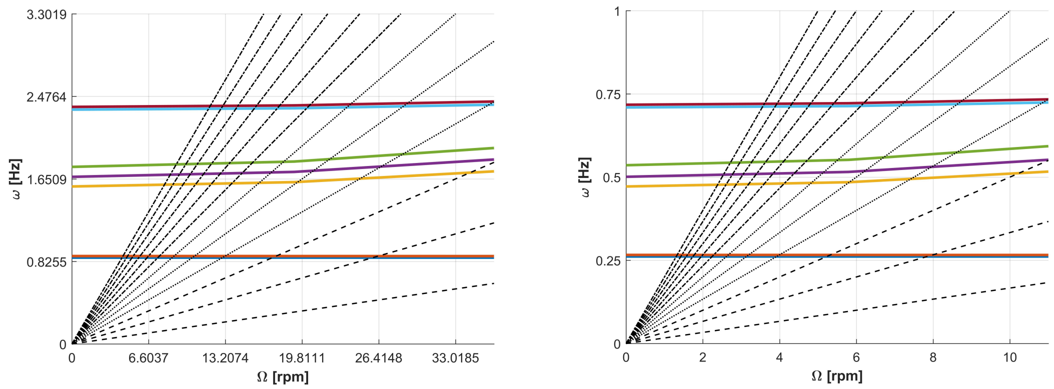

(a) Z-Model (b) 10 MW Model

Figure 5.5: Comparison of the Campbell diagram of the 10 MW Model and the Z-Model

5.2.1 Model set-up

This model can be understood as a reblading of a reference modern-size wind turbine, the 700 kW machine described in Chapter 4.2. Therefore, several macroparameters, such as those listed in Table 5.3, must remain constant. Among these, the hub height of 73 m, or the rotor overhang and root flange stand out.

Data	Value	Data	Value
Wind class	IEC 3A	Rated mech. power	700.00 kW
Hub height	73.00 m	Rotor diameter	54.0 m
Rotor overhang	3.07 m	Length Blade Root Flange	0.65 m

Table 5.3: O-Model main characteristics

However, the blade shape is only constraint by the rotor diameter of 54 m and the airfoils chosen.

Airfoils choice

For the choice of airfoils, the expected Reynolds number of the sub-scale model must be considered. The small rotor dimensions suggest the necessity of airfoils that present a good behavior at low Reynolds numbers. Therefore, six airfoils of different families with relative thicknesses from 40.1 % to 18.0 % have been elected for this design. Their shapes are shown in Figure 5.6.

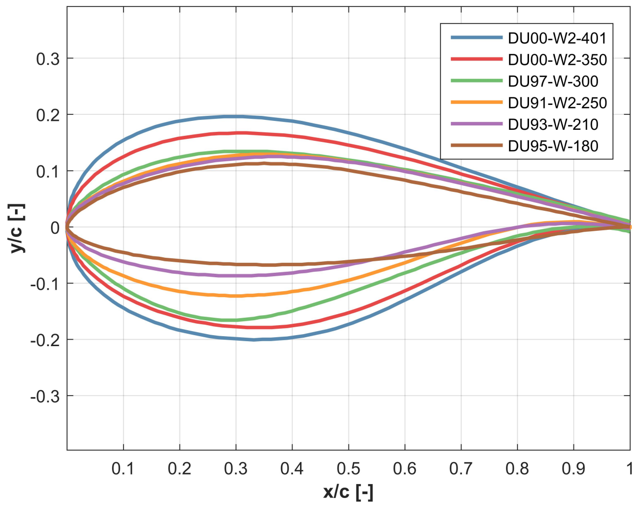

Figure 5.6: Geometry of the airfoils chosen for the O-Model

The aerodynamic properties of these airfoils are computed at Reynolds number around $Re = 3 \times 10^6$ and displayed in Figure 5.7.

5.2.2 Model optimization

The O-Model was thus obtained from the constrained aerodynamic and structural optimization performed in Cp-Max. In this case, only one iteration of each optimization has been performed, being the results presented as follows.

The obtained chord and twist distribution are represented in Figure 5.8.

These are obtained from the optimization of the Cp in Region 2. Its value of 0.4859 is displayed in Table 5.4, being 5.17 % higher than the Cp of the 10 MW machine. The TSR in Region 2 of the new model is equal to the full-scale model because of the constraints set.

Data	10 MW	Z-Model
TSR [-]	7.684	
Pitch [deg]	0.0055	
Cp [-]	0.4620	0.4859
Ct [-]	0.7916	0.8178

Table 5.4: Comparison between Region 2 in the 10 MW model and in O-Model

Furthermore, the O-Model presents a circulation very close to the 10 MW one, as shown in Figure 5.9. The maximum point, located at a nondimensional blade span of 0.3 perfectly fits the reference, while larger differences can be observed in the middle blade span area. These differences are partly caused by an incomplete fulfillment of the circulation constraint during

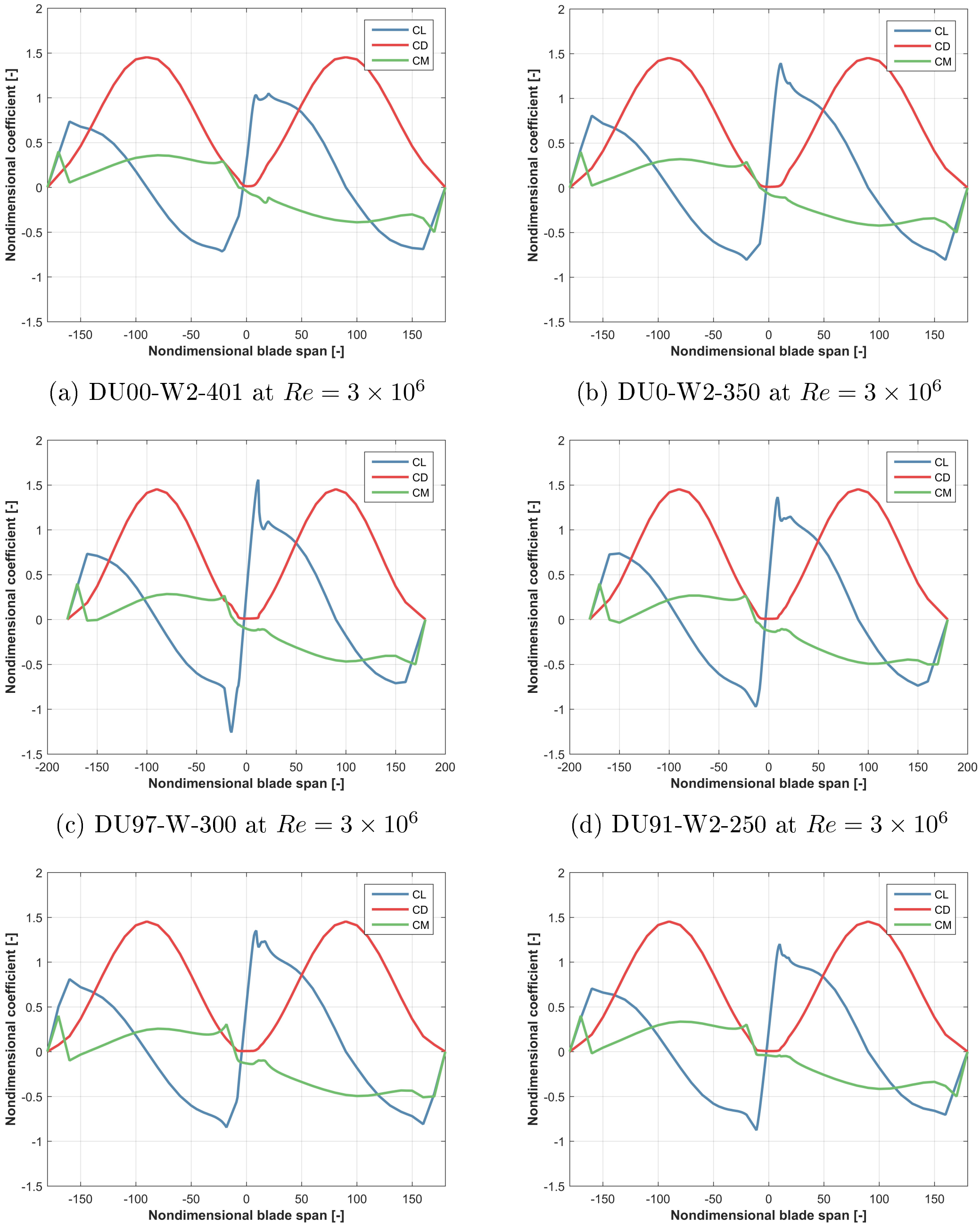

(a) DU00-W2-401 at $Re = 3 \times 10^6$

(b) DU0-W2-350 at $Re = 3 \times 10^6$

(c) DU97-W-300 at $Re = 3 \times 10^6$

(d) DU91-W2-250 at $Re = 3 \times 10^6$

(e) DU93-W-210 at $Re = 3 \times 10^6$

(f) DU95-W-180 at $Re = 3 \times 10^6$

Figure 5.7: Aerodynamic properties of the different airfoils implemented in the O-Model

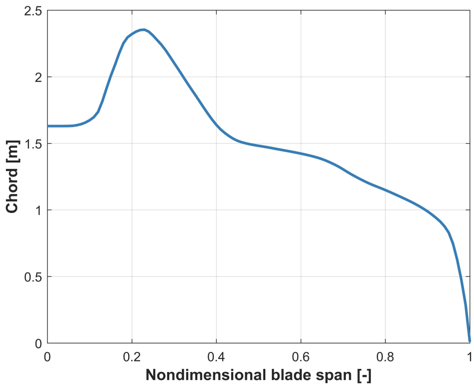

(a) Chord distribution

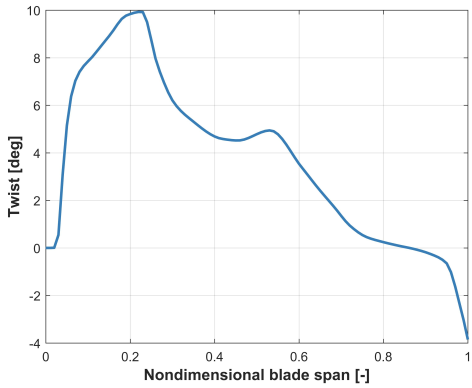

(b) Twist distribution

Figure 5.8: Chord and twist distribution along the model blade

the aerodynamic optimization considering a rigid structure; as well as the mismatching of the structural properties.

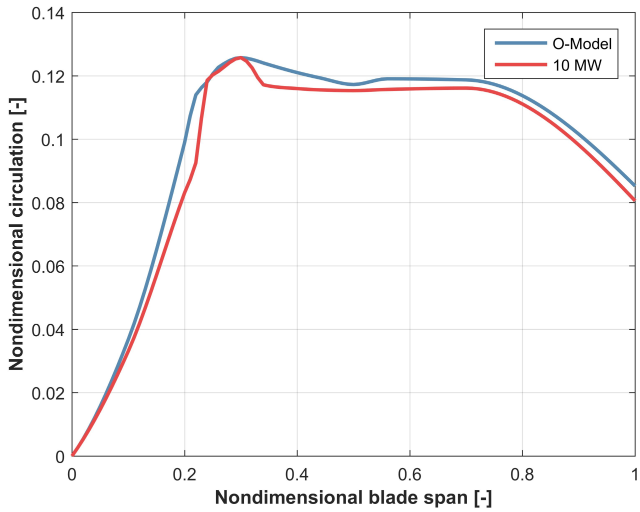

Figure 5.9: Comparison of the circulation in Region 2 of the O-Model and the 10 MW model

On the structural side, the elastic forces are constrained by matching the tip deflection given a certain force. This leads to the partial matching of the elastic forces, as shown in Figure 5.10. The O-Model follows the same trend as the 10 MW model, however presenting some differences.

Inertial forces are modified by matching the first flapping and lagging mode, which leads to strong differences in the Campbell diagram, as deducted from Figure 5.11. The large differences in the tower characteristics introduce important differences in the behavior of the rotor as a whole.

These inaccuracies in the structure, as well as an incomplete fulfillment of the circulation constraint during the aerodynamic optimization justify the partial matching of dynamic behavior of the O-Model.

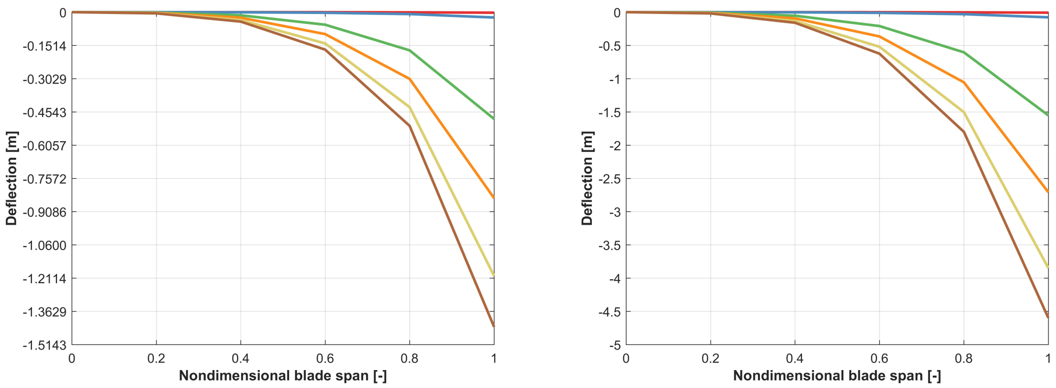

(a) O-Model (b) 10 MW Model

Figure 5.10: Comparison of the deflections of the 10 MW Model and the O-Model

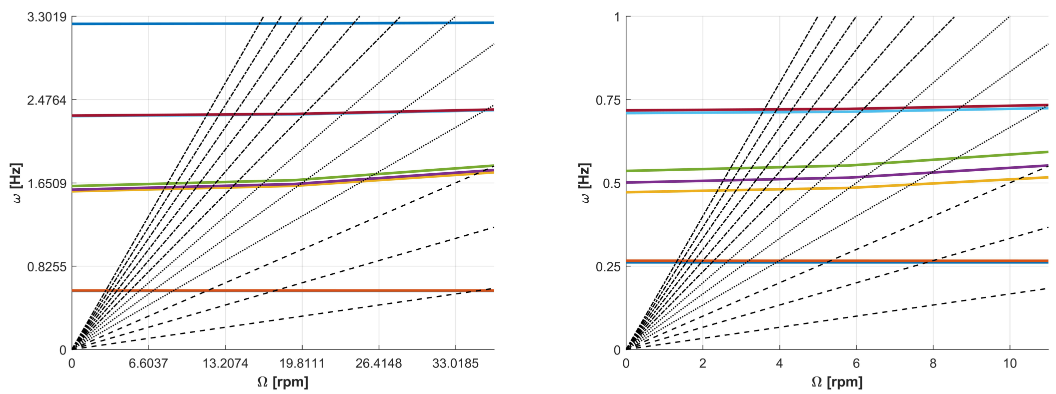

(a) O-Model (b) 10 MW Model

Figure 5.11: Comparison of the Campbell diagram of the 10 MW Model and the O-Model

Chapter 6

Comparison and discussion

In this chapter the aerodynamic and structural characteristics of the sub-scale models will be compared. The feasibility of the models will be also discussed, to determine which approach presents the most promising future perspectives.

6.1 Models overview

In spite of presenting very different characteristics, both Z- and O-Model are capable of reflecting the dynamic behavior of a very large wind turbine. For example, the Z-Model has a hub height of 119.0 m due to its down-zooming nature; while the O-Model has maintained the hub height of the reference modern-size wind turbine. The rotor overhang and cone angle, as well as the nacelle uptilt or the length blade root flange also differ because of this reason. These inequalities, as well as the different chord and twist distribution, and the different set of airfoils implemented lead to divergences in solidity and Cp.

Features	10 MW	700 kW	Z-Model	O-Model
Rotor diameter [m]	178.3	54.0	700 kW	
Hub height [m]	119.0	73	Zoomed	
Rotor cone angle [deg]	4.65	2.5	10 MW	700 kW
Rotor overhang [m]	7.07	3.07	Zoomed	
Length Blade Root Flange [m]	2.80	0.65	Zoomed	
Solidity [%]	4.68		4.68	5.23
Chord			Zoomed	Optimized
Twist			10 MW	Optimized
Airfoils			10 MW	New
Cp (Region 2)	0.4620	-	0.4621	0.4859
Ct (Region 2)	0.7916	-	0.7911	0.8178

Table 6.1: Overview into the characteristics of the full- and sub-scale models

6.2 Aerodynamic characteristics

The chord distribution follows a similar trend in both models, being slightly higher in the O-Model to maximize its Cp. The twist distribution presents larger differences, as the O-Model requires an unsteadier twist to be able to match the set conditions. These trends can be observed in Figure 6.1.

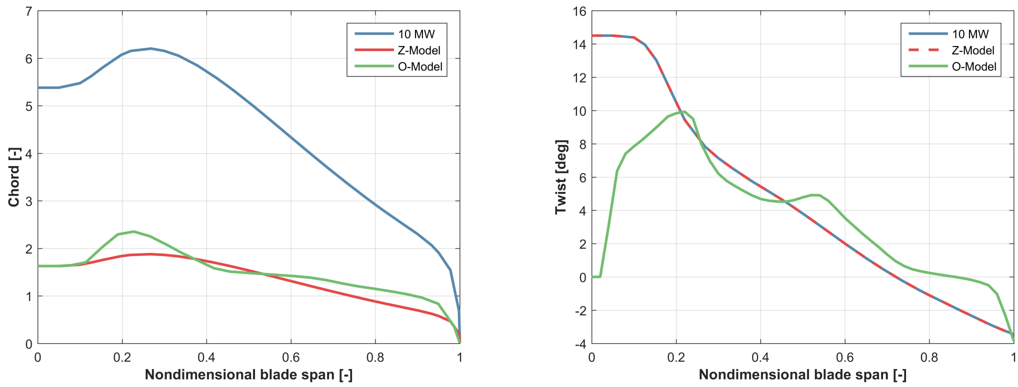

(a) Chord (b) Twist

Figure 6.1: Models comparison

The Mach number can be neglected in both models, as the small rotor dimensions ensures the incompressibility of air. The Reynolds number, whose distribution over the nondimensional blade span is represented in Figure 6.2, presents the same magnitude in both models.

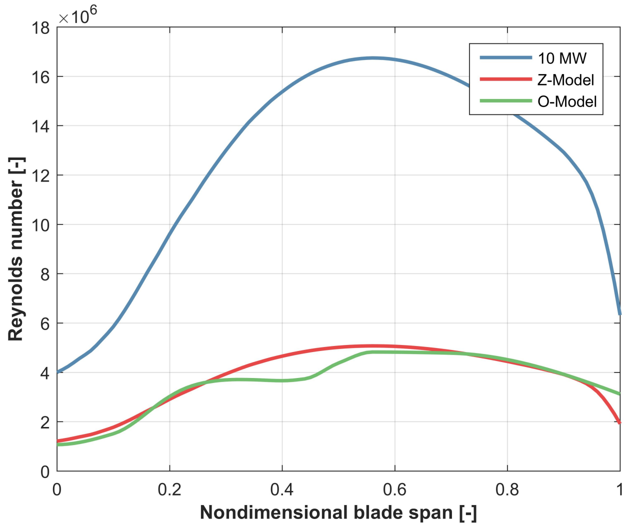

Figure 6.2: Comparison of the Reynolds number of the Z- and the O-Model

The O-Model has been designed with airfoils properly chosen for their performance at this Reynolds number, as commented in Chapter 5.2.1; the Z-Model, on the other hand, has been defined with the same airfoils as the 10 MW model. The airfoil simulation code XFOIL [8] has been thus implemented to acquire a first look into the Reynolds dependency of the airfoils and its effect on the dimensionless circulation. The code shows an adequate predictability of the airfoil performance in the linear regime, while its behavior after stall is not . The evaluation of the predictions accuracy can be found in Appendix A
XFOIL was implemented to compute the properties of all airfoils at a Reynolds number of $Re = 3 \times 10^6$. To account for possible divergences with the data set supplied by by DTU [9] and implemented in this model, these properties were also computed at the Reynolds number of $Re = 1 \times 10^7$. These were extrapolated to the whole angle of attack range by applying the Viterna extrapolation method with the Airfoilprep [25] workbook.

The airfoils were found to show a dependency on the Reynolds number after stall, not changing their behavior in the linear regim. The Reynolds-dependency of the tip airfoil is exhibited in Appendix B to exemplify these changes.

The dimensionless circulation at different Reynolds number is represented in Figure 6.3. The comparison between the circulation distribution computed with the airfoil properties at different Reynolds number predicted by XFOIL suggest slight changes near the root.

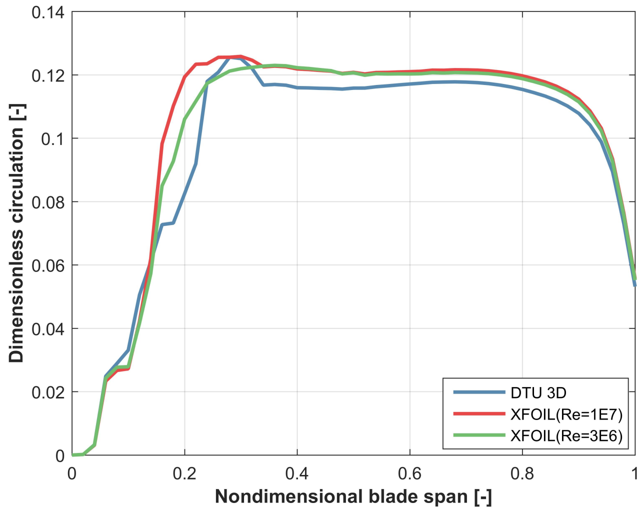

Figure 6.3: Comparison of the dimensionless circulation of the Z-Model given different Reynolds numbers

Therefore, despite presenting the same airfoils, different dimensionless circulations can be obtained, hindering the fulfillment of this scaling law.

6.3 Structural characteristics

Multiple differences between the models structural components can also be observed. These lie on the model design approach, as the Z-Model presents the same structural components as its full-scale counterpart with a scaled thinness, while the structure of the O-Model has been specifically designed.

From the Z-Model structure, represented in Figure 6.4a, the very thin skin at the root stands out, as well as the presence of a third web and root reinforcement. The thinness of these components calls its manufacturing feasibility into question.

On the other side, the O-Model has been design to disregard root reinforcement and third web, avoiding this problem. Furthermore, the root skin requires a much higher thickness.

Regarding the core structure (Figure 6.5), important differences can also be noticed. The trailing edge shell, both for suction and pressure sides requires lower thicknesses than for the O-Model.

The O-Model structure ensures the capability of supporting the loads that the wind turbine will have to face over its lifetime. In this case, only the basic dynamic loads cases (DLC1.1) have been considered. The Z-Model structure fails in supporting those loads. As shown in Figure 6.6, the model would require a much higher shell at the pressure side of the trailing edge.

Therefore, even though both structures success in reflecting the inertial and elastic behavior of the 10 MW machine, the Z-Model presents some issues that may complicate its manufacturing and correct performance.

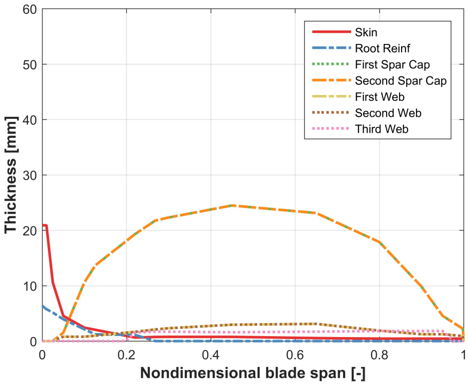

(a) Z-Model

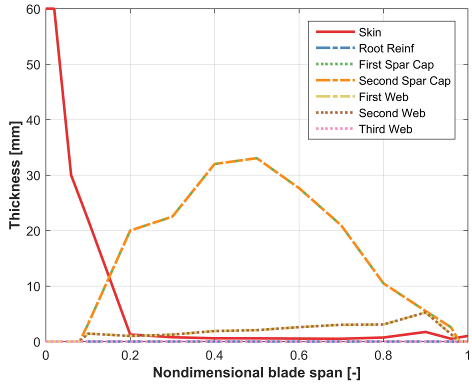

(b) O-Model

Figure 6.4: Comparison of the skin structural thickness

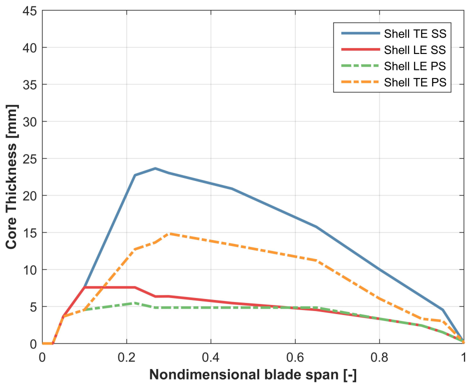

(a) Z-Model

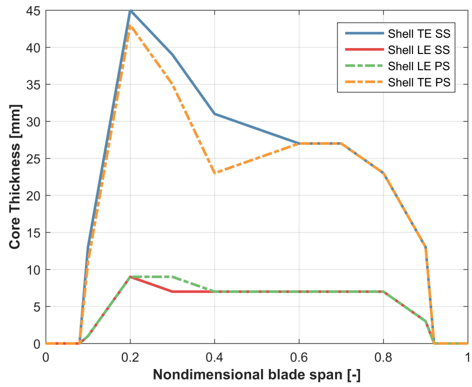

(b) O-Model

Figure 6.5: Comparison of the core structural thickness

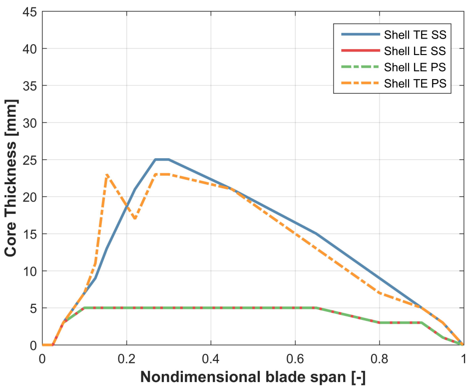

(a) DLC1.1

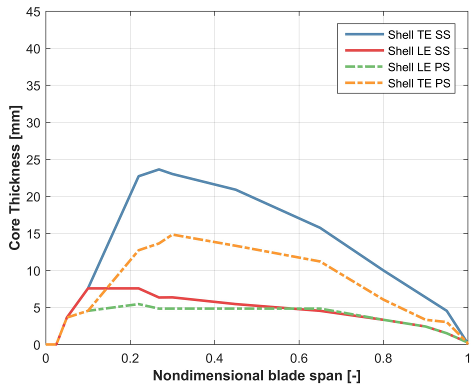

(b) Zoomed structure

Figure 6.6: Comparison between the core structural thickness of the Z-Model and the predicted by the DLC 1.1 cases

Chapter 7

Conclusion and outlook

This thesis focused on the adaptation of the wind turbine design and simulation tool Cp-Max for the design of sub-scale machines capable of replicating the dynamic behavior of very large wind turbines.

To this end, scaling laws were formulated. These are based on non-dimensional parameters relevant to the dynamic behavior of a wind turbine, derived thanks to the Buckingham theorem. Therefore, the fulfillment of the following conditions ensures the reflection of the full-scale dynamic behavior

- The TSR must be kept constant to ensure the same kinetic behavior.
- Dimensionless circulation must remain constant to match the wake.
- The sub-scale model eigenfrequencies must be correspondingly scaled to lock the elastic to inertial forces ratio.
- The sub-scale model blade deflection must correspond to the full-scale ones to allow the same ratio between aerodynamic and elastic forces.

New constraints representing these laws were included in the Cp-Max environment. The aerodynamic optimization loop was subsequently set to determine the chord and twist given certain airfoils and a certain relative thickness distribution that offer the maximum Cp. This algorithm was then constrained to ensure that the optimal solution also presented the desired dimensionless circulation at a given TSR.
The matching of the first flapping and lagging mode, as well as the tip deflection were added to the already existing constraints in the structural loop. Therefore, the code was set to find the optimal thicknesses of the components that respect these constraints and correctly resists the loads of the basic dynamic load cases (DLC 1.1).
Moreover, this new environment was implemented for the exploration and comparison of two different approaches to obtain a sub-scale model behaving like a full-scale wind turbine: a method grounded on the down-zooming of a very large wind turbine (Z-Model), and another based on the redesign of a moderate-size wind turbine (O-Model).

The so-called Z-Model was designed as a scaled replica of a 10 MW wind turbine. The similarity between models was accomplished by the implementation of a time, length and mass scaling ratio, which relates the sub-scale model with the full-scale model characteristics. The method succeeded in achieving a sub-scale model capable of perfectly reproducing the dynamic behavior of its full-scale counterpart, as the same TSR, dimensionless circulation, Campbell diagram and blade deflections were observed.
However the feasibility of this model is questioned: the zoomed-down nature of this approach requires the implementation of the same airfoils and the reduction of structural thicknesses, which may lead to aerodynamic and structural issues.
On the one side, the Reynolds number of the sub-scale model largely differs from the full-scale model one, resulting in different operating conditions for the same airfoils. This may generate

a different behavior of the airfoils, as their properties depend on the Reynolds number. On the other side, very thin structural components result of the scaling of the very large wind turbine. The manufacturing of such thin skins, root Moreover, the scaling of extra non-structural masses, such as the lightning system or glues is required for a correct behavior of the machine. This approach, nevertheless, may not be feasible, being not possible to achieve it.

The O-Model was created as a redesign of a 700 kW machine to present the same dynamic behavior as a 10 MW machine. The constrained aerodynamic and structural optimization algorithms were applied, achieving a design showing an optimum Cp and blade cost. The model could be tailored to present realistic characteristics. An adequate set of airfoils was implemented, as well as the presence of a root reinforcement and third web were avoided.
The dynamic behavior, however, just partially matches its full-scale counterpart. The partial fulfillment of the dimensionless circulation constraint, as well as the restricted formulation of the structural constraints can be pointed out to justify it.

Therefore, both models present issues that question their suitability. The main difference lies on the future perspectives. The questions raised in the Z-Model, including the airfoil performance at lower Reynolds number and the potential manufacturing problems represent important issues that can not be handled. The large tightness of the approach does not provide any degree of freedom to face these problems.
However, the flexibility of the redesign approach offers alternatives to gain a better fulfillment of the full-scale model behavior. The inclusion of more constraints into the Cp-Max environment will allow a higher similarity in inertial and elastic forces, while through the re-optimization of the aerodynamic features, the complete matching of the dimensionless circulation can be achieved.

Appendix A

XFOIL Validation

The validation of this tool can be carried out by comparing the aerodynamic properties predicted by this code with the ones established in wind tunnel tests. Therefore the airfoils $NACA63_{(2)} - 615$ and $NACA63_{(4)} - 221$ are adequate as their aerodynamic properties were set in wind tunnel tests performed by the National Advisory Committee for Aeronautics in 1945. These properties can be found at different Reynolds numbers in [7] and will serve as a reference to validate the XFOIL predictions. The airfoils $NACA63_{(2)} - 615$ and $NACA63_{(4)} - 221$, whose shapes are represented in Figure A.1, have been chosen due to the similar relative thickness to the ones that can be currently found on the outer part of wind turbines.

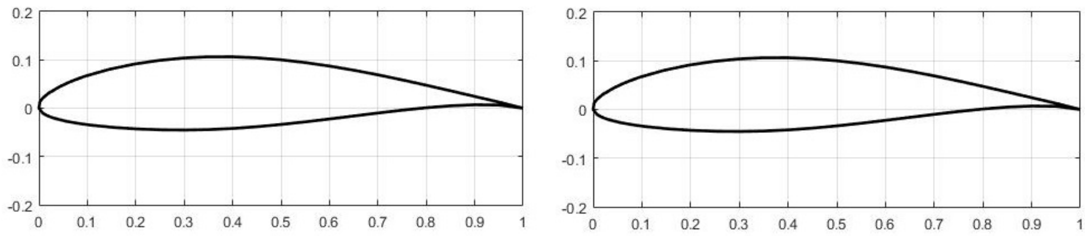

(a) NACA63(2)-615 (b) NACA63(4)-221

Figure A.1: Airfoils chosen for the XFOIL validation

The CL and CD behavior of the $NACA63_{(2)} - 615$ and the $NACA63_{(4)} - 221$ airfoils at different Reynolds number are represented in Figure A.2 and Figure A.3 respectively. On the one side, CL follows the same tendency in both airfoils, showing small differences in the linear regime between the CL curves predicted by XFOIL and the ones experimentally established at different Reynolds numbers.

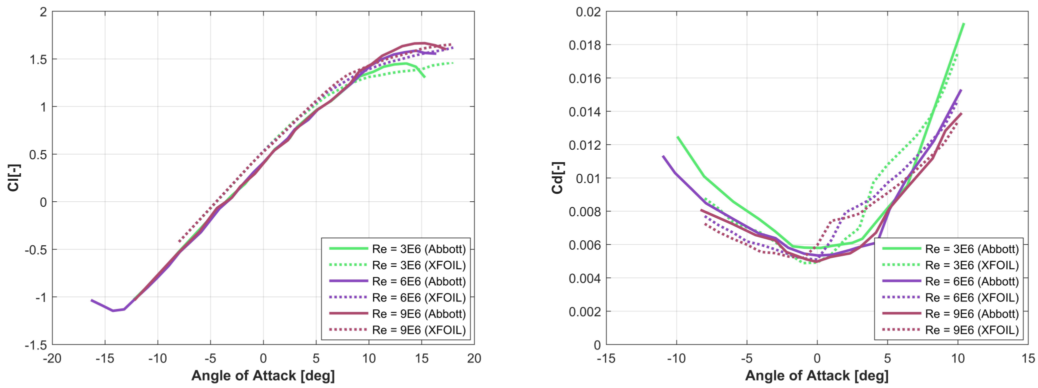

(a) CL (b) CD

Figure A.2: $NACA63_{(2)} - 615$ aerodynamic properties established in wind tunnel test (Abbott [7]) or computed by XFOIL [8]

However it is unable to accurately predict the real aerodynamic properties after stall. CD, on the other side, presents more notorious differences between the airfoil properties at the same Reynolds number. Therefore it can be concluded that the airfoil properties predicted by XFOIL may present some significant divergences in comparison to the experimental ones, so its implementation should be carefully performed.

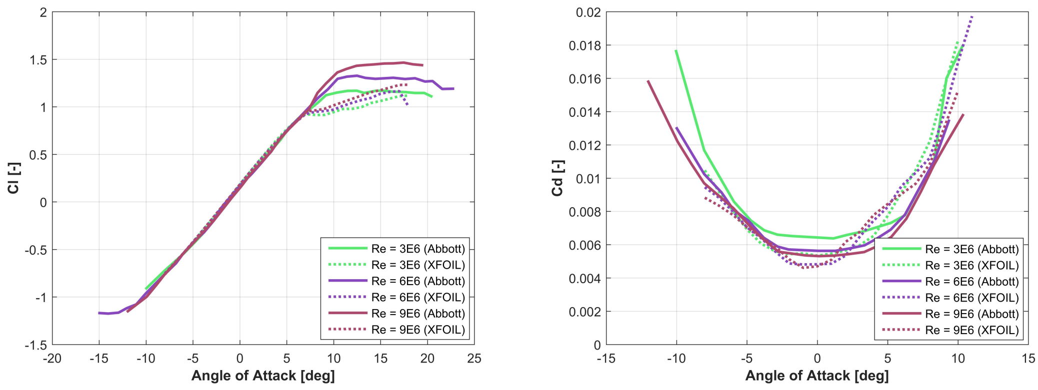

(a) CL (b) CD

Figure A.3: $NACA63_{(4)}-221$ aerodynamic properties established in wind tunnel test(Abbott [7]) or computed by XFOIL [8]

Appendix B

Reynolds number dependency

The FFA-W3-241 airfoil, whose geometry is displayed in Figure B.1 has been chosen to represent the comparison between all airfoils. It is thinnest airfoil in the model, so it is most likely to present a better behavior than the airfoils implemented near the root.

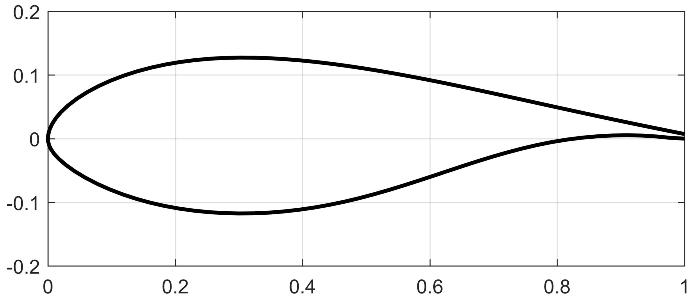

Figure B.1: Geometry of the FFA-W3-241 airfoil

The comparison between the airfoil properties predicted by XFOIL [8] and computed by DTU [9] shows that the XFOIL prediction follows the same trend as the DTU data, but with differences in the stall region.

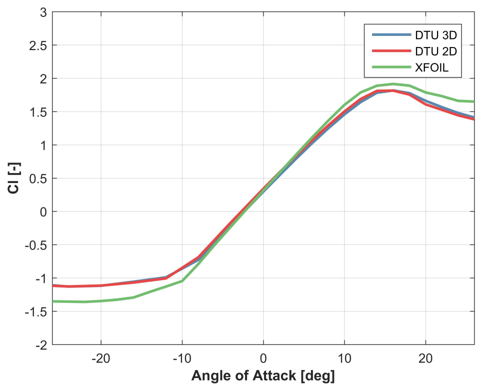

(a) CL at $Re = 1.2 \times 10^7$

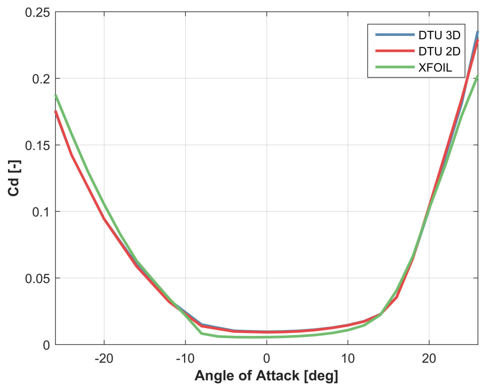

(b) CD at $Re = 1.2 \times 10^7$

Figure B.2: Comparison of the FFA-W3-241 airfoil properties given the data in DTU [9] and computed with XFOIL [8]

The Reynolds-dependency of the behavior of the Cl given different Mach numbers is exhibited in Figure B.3. From these figures it can be concluded, that the CL presents a similar behavior at different Reynolds number in the linear regime, while it shows a different pattern at stall conditions. The negligibility of the Mach number is also made clear, as the incompressibility of the flow in all cases is ensured, being this number low enough.

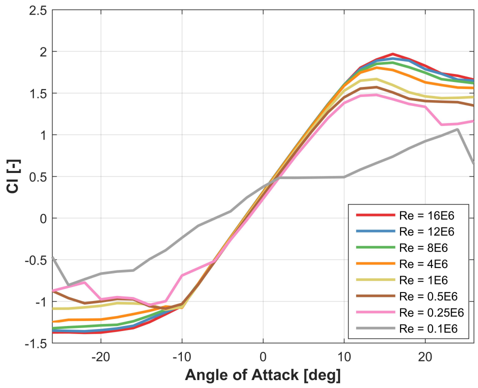

(a) Ma = 0.26

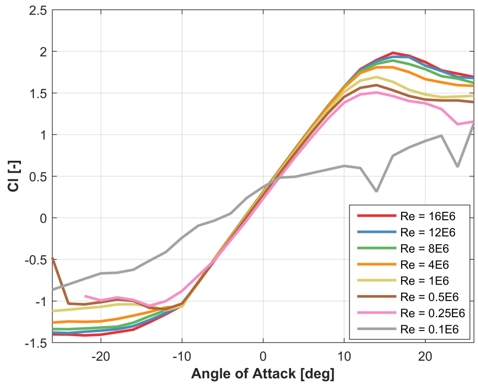

(b) Ma = 0.22

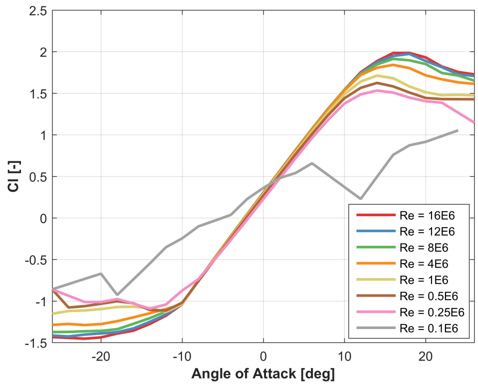

(c) Ma = 0.15

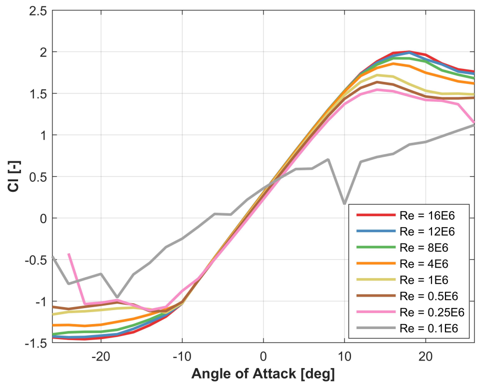

(d) Ma = 0.1

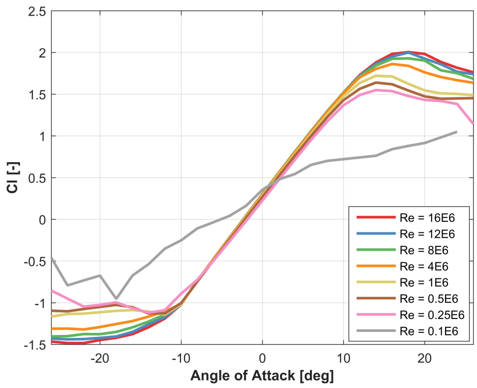

(e) Mach = 0.05

Figure B.3: Reynolds dependency of the FFA-W3-241 airfoil at different Mach numbers computed by XFOIL [8]

.

[1] GWEC, "Global wind report: Annual market update," 20156.

[2] C. L. Bottasso, F. Campagnolo, and V. Petrović, "Wind tunnel testing of scaled wind turbine models: Beyond aerodynamics," *Journal of Wind Engineering and Industrial Aerodynamics*, vol. 127, pp. 11 – 28, 2014. [Online]. Available: http://www.sciencedirect.com/science/article/pii/S0167610514000269

[3] EWEA, "Upwind: Design limits and solutions for very large wind turbines," 2011.

[4] S. N. Laboratories, "Swift commissioned to study wind farm optimization," July 2013. [Online]. Available: https://share-ng.sandia.gov/news/resources/news_releases/swift-wind-farm-optimization/#.WKBMpW_hDIU

[5] B. R. Resor and D. C. Maniaci, *Definition of the National Rotor Testbed: An Aeroelastically Relevant Research-Scale Wind Turbine Rotor*, Dec 2013. [Online]. Available: http://www.osti.gov/scitech/servlets/purl/1124217

[6] P. Bortolotti, C. L. Bottasso, and A. Croce, "Combined preliminary–detailed design of wind turbines," *Wind Energy Science*, vol. 1, no. 1, pp. 71–88, 2016. [Online]. Available: http://www.wind-energ-sci.net/1/71/2016/

[7] I. Abbott, A. von Doenhoff, and L. Stivers, *Report No. 824: Summary of airfoil data*. National Advisory Committee for Aeronautics, 1945.

[8] M. Drela and H. Youngren, *XFOIL, v. 6.99*, 2013.

[9] C. Bak, F. Zahle, R. Bitsche, T. Kim, A. Yde, L. Henriksen, P. Andersen, A. Natarajan, and M. Hansen, *Design and performance of a 10 MW wind turbine*. Wind Energy, to be accepted.

[10] T. NORD, *GARUDA 700.54, EU54.1250.1-B, HH 73 m : Design Evaluation Conformity Statement*, 2013.

[11] L. Vermeer, J. Sørensen, and A. Crespo, "Wind turbine wake aerodynamics," *Progress in Aerospace Sciences*, vol. 39, no. 6–7, pp. 467 – 510, 2003. [Online]. Available: http://www.sciencedirect.com/science/article/pii/S0376042103000782

[12] D. Simms, S. Schreck, M. Hand, and F. L.J., "Nrel unsteady aerodynamics experiment in the nasa-ames wind tunnel: A comparison of predictions to measurements," June 2001.

[13] C. Bottasso and A. Croce, *Cp-Lambda: User's Manual*. Dipartimento di Scienze e Tecnologie Aerospaziali, Politecnico di Milano, 2006-2014.

[14] C. L. Bottasso, F. Campagnolo, and A. Croce, "Multi-disciplinary constrained optimization of wind turbines," *Multibody System Dynamics*, vol. 27, no. 1, pp. 21–53, 2012. [Online]. Available: http://dx.doi.org/10.1007/s11044-011-9271-x

[15] C. L. Bottasso, P. Bortolotti, A. Croce, and F. Gualdoni, "Integrated aero-structural optimization of wind turbines," *Multibody System Dynamics*, vol. 38, no. 4, pp. 317–344, 2016. [Online]. Available: http://dx.doi.org/10.1007/s11044-015-9488-1

[16] MATLAB, *version 9.10.0 (R2016a)*. Natick, Massachusetts: The MathWorks Inc., 2016.

[17] *Wind Turbines - Part 1 : Design Requirements, Ed. 3*, 2005th ed. International Standard IEC 61400-1, 2005.

[18] *Guideline for the Certification of Wind Turbines*, 2010th ed. Brooktorkai 10, 20457 Hamburg, Germany: Germanischer Lloyd Industrial Services GmbH, Renewables Certification, 2010.

[19] N. I. Portal, *TurbSim v1.40*, 2016. [Online]. Available: https://nwtc.nrel.gov/TurbSim

[20] V. Giavotto, M. Borri, P. Mantegazza, and G. Ghiringhelli, "Anisotropic beam theory and applications," *Computers & Structures*, vol. 16, no. 1, pp. 403 – 413, 1983. [Online]. Available: http://www.sciencedirect.com/science/article/pii/0045794983901797

[21] E. Buckingham, "On physically similar systems; illustrations of the use of dimensional equations," *Phys. Rev.*, vol. 4, pp. 345–376, Oct 1914. [Online]. Available: http://link.aps.org/doi/10.1103/PhysRev.4.345

[22] A. Hassanzadeh, J. W. Naughton, C. L. Kelley, and D. C. Maniaci, "Wind turbine blade design for subscale testing," *Journal of Physics: Conference Series*, vol. 753, no. 2, p. 022048, 2016. [Online]. Available: http://stacks.iop.org/1742-6596/753/i=2/a=022048

[23] J. F. Manwell, J. G. McGowan, and A. L. Rogers, *Wind energy explained : theory, design and application*. Chichester: Wiley, 2009. [Online]. Available: http://opac.inria.fr/record=b1130703

[24] C. Bak and P. B. Andersen, "Three-dimensional corrections of airfoil characteristics based on pressure distributions."

[25] N. I. Portal, *Airfoilprep v2.02.03*, 2014. [Online]. Available: https://nwtc.nrel.gov/AirFoilPrep